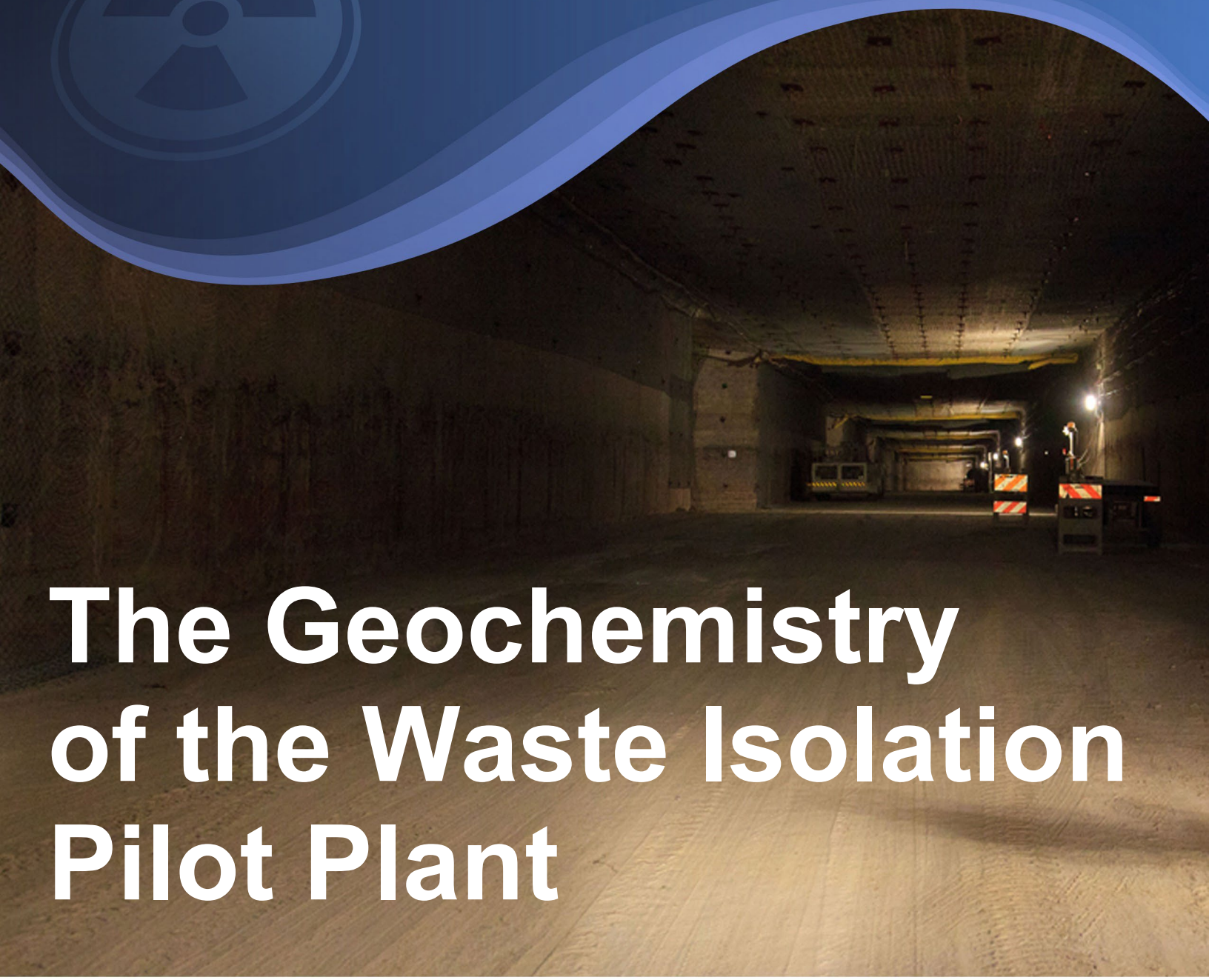

The Geochemistry of the Waste Isolation Pilot Plant

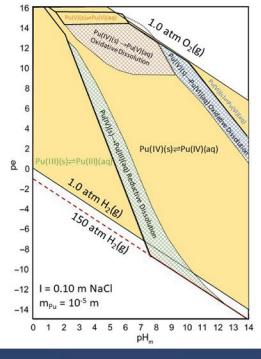

EPA-402/R-21/002 | November 2021
https://www.epa.gov/radiation/epas-role-waste-isolation-pilot-plant-wipp

Preface

The Waste Isolation Pilot Plant (WIPP), located near Carlsbad, New Mexico, is a deep geologic repository for the disposal of defense-related transuranic radioactive waste operated by the U.S. Department of Energy (DOE). The repository is located in a bedded salt deposit, approximately 660 meters below the subsurface. Regulatory oversight for the radioactive waste at the facility is provided by the U.S. Environmental Protection Agency (EPA) as established by the WIPP Land Withdrawal Act. As a part of a demonstration of compliance with radioactive waste disposal standards that EPA has established, DOE submits a Performance Assessment (PA) model calculation for the repository's 10,000-year regulatory timeframe. This PA calculation projects potential quantities of actinides released into the accessible environment as a result of various potential intrusions into the repository. EPA initially certified the WIPP's compliance in 1998, and since the facility first received waste in 1999, DOE has submitted a recertification application with an updated PA every 5 years.

The PA incorporates multiple different models and concepts, ranging from the rock mechanics of the surrounding salt matrix to the geochemistry of the actinides' interacting with brine pockets. This document provides an overview of the various geochemical concepts in the PA used to estimate actinide releases and relates them to the specific conditions at the WIPP and the PA methods. The various sections in the document are meant to be modular and can be used separately or in conjunction with the rest of the document as a primer to give context and background to different models present in the PA.

Acknowledgements

Eugenio Felipe Unson Santillan from the Office of Air and Radiation's (ORIA) Radiation Protection Division was the principal author of this work.

EPA and ORIA would like to thank the following people for their assistance, input, and technical reviews of the various drafts of this document:

Gary Chen, U.S. EPA, Office of Radiation and Indoor Air, Office of Air and Radiation
Philip Flanders, U.S. EPA, Office of Science and Technology, Office of Water
Hannah Leigh, U.S. EPA, Office of Radiation and Indoor Air, Office of Air and Radiation
Jonathan Major, U.S. EPA, Office of Radiation and Indoor Air, Office of Air and Radiation
Danny Malashock, U.S. EPA, Office of Radiation and Indoor Air, Office of Air and Radiation
Tom Peake, U.S. EPA, Office of Radiation and Indoor Air, Office of Air and Radiation
Kayla Reiser, U.S. EPA, Office of Radiation and Indoor Air, Office of Air and Radiation
Joe Rustick, U.S. EPA, Office of Radiation and Indoor Air, Office of Air and Radiation
Janet Schramke, SC&A, Inc.
Dan Schultheisz, U.S. EPA, Office of Radiation and Indoor Air, Office of Air and Radiation
Dave Stuenkel, U.S. EPA, Office of Radiation and Indoor Air, Office of Air and Radiation
Xinyue Tong U.S. EPA, Office of Radiation and Indoor Air, Office of Air and Radiation

Contract support was provided by Marisa Thornton and Jessica Wieder, U.S. EPA, Office of Radiation and Indoor Air, Office of Air and Radiation. Both technical and graphics editing were provided by Ellen Wang, U.S. EPA, Office of Radiation and Indoor Air, Office of Air and Radiation, as well as The Scientific Consulting Group, Inc.

Cover images were sourced from the DOE WIPP website (https://wipp.energy.gov/) and from this document. Images consist of a WIPP tunnel (https://wipp.energy.gov/WIPPCommunityRelations/images/photos/UG.jpg), a plutonium stability diagram (Figure 6-2), a salt crystal (https://wipp.energy.gov/geologic-disposal-safety-case.asp), and an aerial view of the WIPP (https://wipp.energy.gov/historytimeline.asp).

Lastly, this project would not have been possible without an opportunity provided by the Presidential Management Fellows Program.

Contents

List of Figures

List of Tables

List of Boxes

1 Introduction

The Waste Isolation Pilot Plant (WIPP) is a deep geologic nuclear waste repository located near Carlsbad, New Mexico, operated by the U.S. Department of Energy (DOE). The facility is located 660 meters below the surface in a geologic formation known as the Salado Formation, which is comprised primarily of bedded salt. The facility is composed of underground tunnels that have been excavated from the salt deposits to create eight waste panels, each with seven rooms (Figure 1-1). Bedded salt within the Salado Formation was chosen specifically because it is free of fresh flowing water, easily mined, geologically stable, impermeable, and able to isolate and encapsulate the radioactive waste over geologic time scales because of salt's ductile properties.

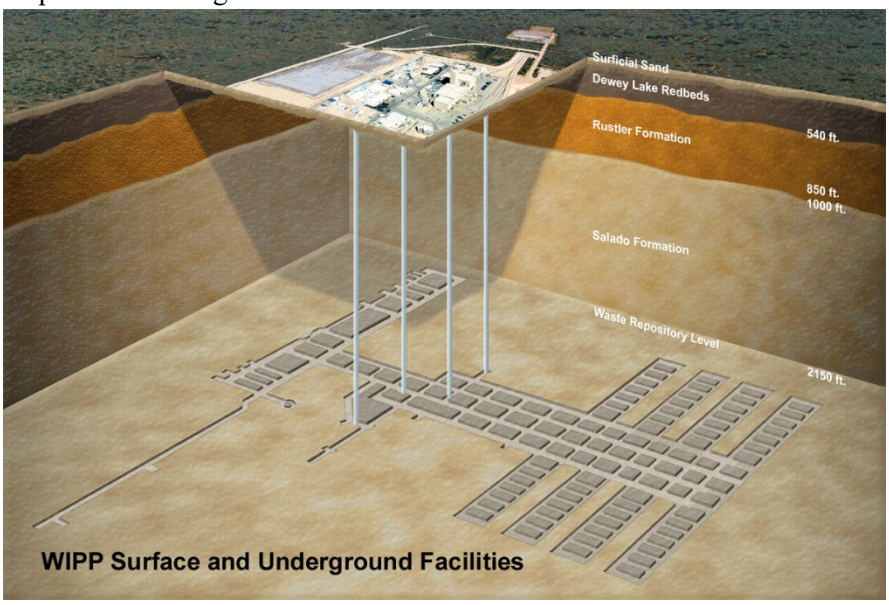

Figure 1-1. Schematic of the WIPP

The facility is designed to isolate defense-related transuranic (TRU) radioactive waste and has a total legislated capacity to dispose of nearly 176,000 cubic meters (6.2 million cubic feet) of waste. TRU waste consists of radioactive elements with high atomic numbers, such as uranium (U), neptunium (Np), plutonium (Pu), americium (Am), curium (Cm), and beyond (also referred to as "actinides"). Wastes are byproducts of nuclear weapons production or cleanup of nuclear weapons production and include contaminated tools, rags, protective clothing, sludges, soil, and other materials. Table 1-1 lists all the non-TRU waste inventory at the WIPP, including the waste containers and the magnesium oxide (MgO) engineered barrier (see Section 4.3.3.2 for more details).

Material	Total (kg)
Iron-Based Metals/Alloys	1.54×10^7
Lead	1.38×10^7
Cellulosics, Plastics, and Rubber	1.11×10^7
Cement	1.76×10^7
Soil	5.01×10^6
Oxyanions (NO_3^-, $SO4^{2-}$, PO_4^{3-})	2.42×10^6
MgO	33,400 tons (Offner 2019)
Organic Ligands	5.54×10^4

Table 1-1. WIPP Waste Inventory (from Van Soest 2018)

Figure 1-2 provides the approximate total inventory of radionuclides in the repository decayed through WIPP's 10,000-year regulatory period. Wastes consist of contact-handled (CH) wastes, which have a radiation surface dose rate of 200 millirem (mrem) per hour or less, as well as remote-handled (RH) wastes with measured surface dose rates up to 1,000 rem per hour.

1.1 EPA's Regulatory Authority

Congress initially authorized the WIPP's development and construction in 1980. It later passed the WIPP Land Withdrawal Act (LWA) in 1992, charging the U.S. Environmental Protection Agency (EPA) with

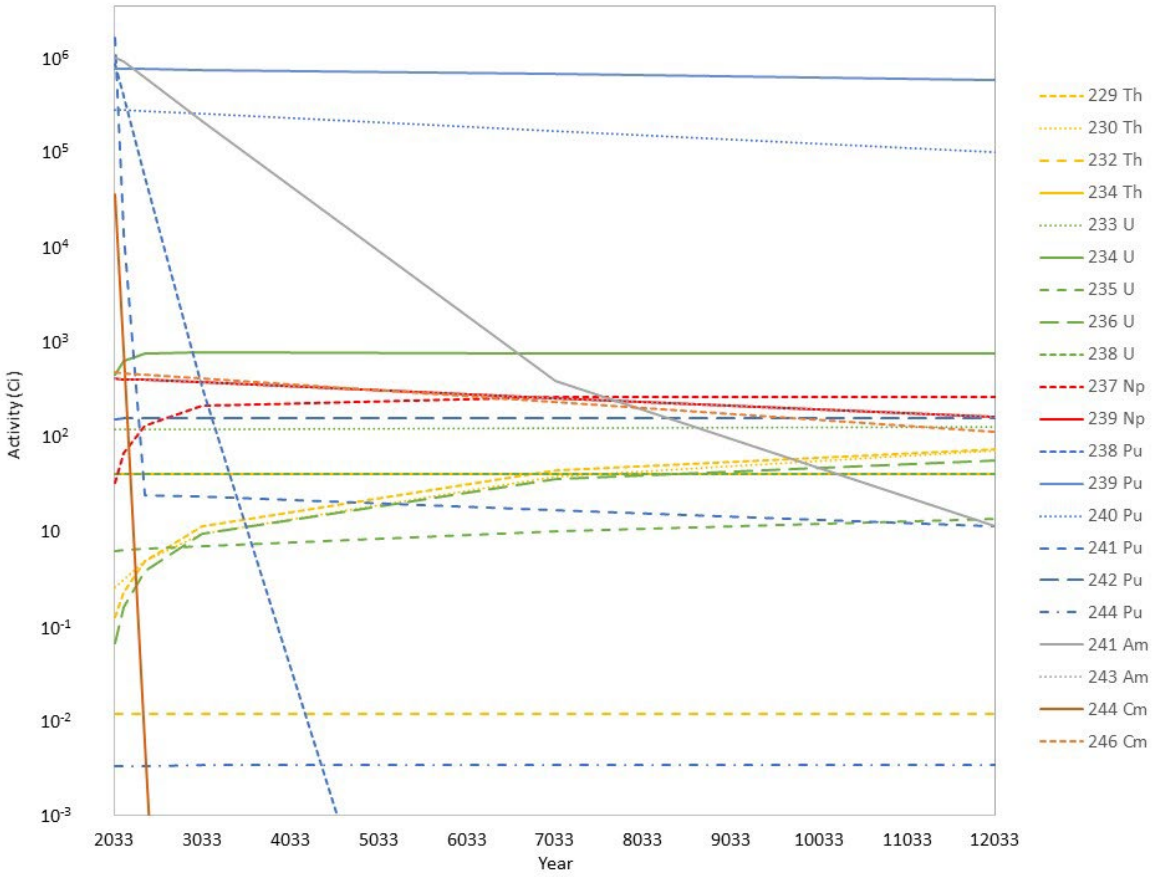

Figure 1-2. WIPP actinide inventory decayed through the year 12033 (from Van Soest 2018)

the authority to develop the radioactive waste disposal standards and certification compliance criteria to apply the standards specifically for the WIPP.[1] The WIPP LWA directs EPA to oversee and regulate the WIPP and includes requirements for EPA to conduct audits and inspections of wastes characterized to be eligible for disposal at the WIPP.

Under this authority, EPA reviewed DOE's compliance certification application (CCA), certified WIPP in 1998, and has reviewed recertification applications (compliance recertification application, or CRA) of the repository every 5 years since March 1999, which was the start of waste handling operations. Additionally, in its applications for certification and recertification, DOE demonstrates compliance with radioactive waste disposal standards through a series of modeling calculations called a Performance Assessment (PA). This assessment contains an analysis that utilizes various models and computer calculations to estimate cumulative releases of radionuclides to the accessible environment over a 10,000-year regulatory period. The PA is a highly technical exercise that incorporates principles of geochemistry and rock mechanics in its assumptions and calculations.

1.2 WIPP Inventory and Engineered Barriers

WIPP's TRU waste sources are derived primarily from plutonium fabrication and reprocessing, research and development, decontamination and decommissioning, and environmental restoration. Some sites that have sent or are currently sending waste to the WIPP include the Hanford Site, Idaho National

[1]See 40 CFR Parts 191 and 194 for more details on EPA's WIPP-specific disposal standards.

Laboratory, Lawrence Livermore National Laboratory, Los Alamos National Laboratory, Oak Ridge National Laboratory, Rocky Flats Environmental Technology Site, and Savannah River Site.

Prior to shipment to the WIPP, waste generator sites characterize the waste and estimate its contents and packaging to provide to the WIPP waste inventory. Inventory data are compiled in the WIPP Waste Data System (WDS), allowing DOE to track the waste estimates. These data, along with estimates provided by the generator sites, are further compiled into the Comprehensive Inventory Database (CID) annually and eventually created into a Performance Assessment Inventory Report (PAIR), which provides the values used for the PA. Current inventory quantities are scaled upward using a scaling factor to assume a repository that has been filled to its legislated capacity. Thus, the inventory values input into the PA (e.g., radionuclides, cements, iron, and lead from the waste containers) are values scaled up from the values found in the CID. Values presented in Table 1-1 and Figure 1-2 are scaled up values from the inventory reports used for the 2019 Compliance Recertification Application.

The radioactive inventory of the WIPP will change over time because of radioactive decay. The WIPP pays specific attention to the actinides that will decay to form alpha-emitting TRU radionuclides with half-lives greater than 20 years, as specified by the LWA. Of the TRU waste identified, the longest-lived radionuclides throughout the repository's life are Pu, Am, and Cm, and these actinides, especially Pu, will dominate potential releases over 10,000 years.

The waste contents and packaging presented in the PAIR provide inputs into the PA, and these contents all will have some influence on the geochemistry. For example, iron-based metals/alloys, lead, and oxyanions will have an impact on redox chemistry (Section 6). Cement may affect solubility and brine pH (Sections 3.3.2 and 4.2.1). Cellulosic, plastic, and rubber (CPR) material will affect gas generation (Section 6.2.1). Soils will affect microbial activity, which will affect redox chemistry and colloids (Sections 5.4.2 and 6.4). The MgO engineered barrier will affect gas chemistry, water balance, and pH through its multiple reactions (Sections 3.3.2 and 4.3.3.2).

2 WIPP Geology

The WIPP is in the Delaware Basin (Figure 2-1), a depositional and structural basin in New Mexico that hosted an ancient shallow sea during the Permian time period (298.9 million years ago). The basin was created by ancient tectonic processes and is composed of a thick succession of sedimentary rocks (up to 200 meters) covered by an exceptionally thick (1,200+ meters) sequence of evaporites (primarily rock salt or halite and anhydrite) from repeated evaporation of that ancient shallow sea. This large salt deposit, which makes it an ideal location to store waste, also contains sizable potash resources (i.e., mined potassium salts used for industrial and agricultural purposes), and abundant hydrocarbons are found in strata below. The WIPP repository itself is located within the Salado Formation, the middle and most halite-rich unit of the larger series of evaporite deposits. Underlying the evaporite deposits are a series of marine sandstones and shales, surrounded by the Capitan carbonate reef, which hosts the famous Carlsbad Caverns. Overlying the evaporite deposits are Triassic and Tertiary sandstones, as well as Quaternary deposits.

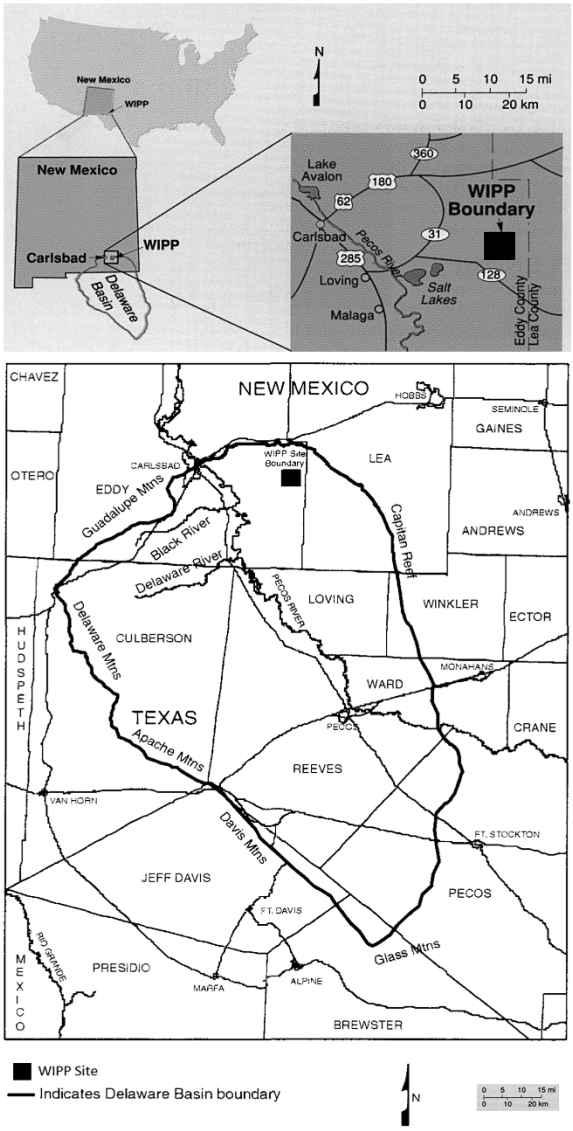

Figure 2-1. The WIPP and its location in the Delaware Basin

2.1 Geologic History

The Delaware Basin is one of the large sub-basins that make up the greater Permian Basin, which was a broad shallow sea 541–323 million years ago. Subsequent tectonic uplift and subsidence across the region resulted in multiple basins within the shallow sea, including the Delaware Basin. The Delaware Basin itself was mostly surrounded by shallow coastal plains with a small inlet south, which provided an occasional supply of seawater to the basin. Over time, during the Permian period, a carbonate reef built up that fringed the Delaware Basin, the most notable reef being the Capitan Reef formation, formed 259–273 million years ago.

During this time, glaciation also caused sea level to drop, eventually cutting the Delaware Basin off from its seawater inputs. The sea eventually disappeared as a result of the continuing deposition of sediment from the shallow coastal plain north of the basin and the evaporation of seawater. This seawater evaporation is responsible for the evaporite sequences found within the WIPP stratigraphy.

2.2 WIPP Stratigraphy

2.2.1 Salado Formation

The WIPP is located approximately 660 meters below the surface in the Salado Formation (Figure 2-1). This geologic unit is composed primarily of halite (NaCl). Interbedded layers of anhydrite ($CaSO_4$), polyhalite ($K_2MgCa_2(SO_4)_4 \cdot 2H_2O$), sylvite (KCl), and mudstone also are present in the unit. Each interbedded layer is referred to as a marker bed (MB), and layers are labeled in the Salado from MB 100

at the top of the formation to MB 144 at the bottom. The origin of the Salado is marine, having formed due to mineral precipitation after the evaporation of the shallow sea discussed earlier.

Small quantities of intragranular and intergranular fluids are present in the salt. Intragranular fluids include fluid inclusions in the Salado, whereas intergranular fluids are fluids located between grain boundaries of the rock. Fractures related to differential stress in the anhydrite layers from plastic flow of halite layers above and below also have resulted in the salt deposit's containing pockets of pressurized brine derived from seawater trapped earlier in its history. Fluid in the Salado is extremely saline (ionic strengths of up to 8 molar) and is represented through the Generic Weep Brine (GWB) brine in the WIPP PA (Table 2-1). GWB is an Na-Cl-type water, although significant amounts of Mg^{2+}, K^{+}, SO_4^{2-}, and borate are present. The composition of this brine was based on analyses of intergranular fluids that seeped into the WIPP excavations.

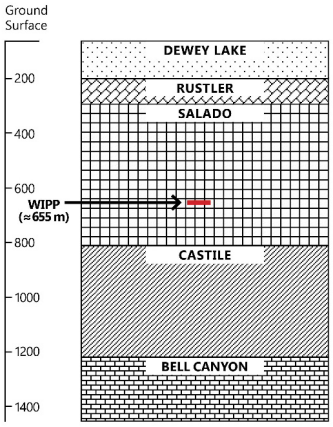

Figure 2-2. Geologic cross-section of the WIPP

2.2.2 Castile Formation

The Castile Formation is an evaporitic deposit that underlies the WIPP and is important because it also contains zones of highly pressurized brine, termed brine pockets, that may enter the repository following a drilling event. At its thickest, the unit is approximately 487 meters and is composed of largely of anhydrite, halite, and some sandstone and limestone. The WIPP PA represents brines in this formation as the ERDA-6 brine, listed in Table 2-1. Waters from this brine may enter the WIPP if drilling penetrates a pressurized brine pocket in this formation (see Section 10.2.3). ERDA-6 brine is an Na-Cl-type water with appreciable amounts of borate, K^{+}, and sulfate (SO_4^{2-}). Brine composition in the WIPP PA is bracketed by the compositions of GWB and ERDA-6.

2.2.3 Rustler Formation

The Rustler Formation overlies the Salado and contains the relatively transmissive Culebra Dolomite, which affects groundwater flow during a potential release because of its highly fractured nature, specifically the variable, nonuniform horizontal and vertical fractures within the unit (see Section 10.2.4).

The WIPP PA includes models to represent actinide sorption onto the dolomite and estimate the potential magnitude of a release. This unit is subject to extensive groundwater monitoring by the WIPP.

As with the Castile and Salado Formations, the Rustler is composed largely of evaporite rocks, although it is more heterogeneous and contains more clastics than others. It is composed of multiple members, including the Lower Rustler, Culebra Dolomite, Tamarisk, Magenta Dolomite, and the Forty-Niner members. The lithology of these members ranges from siltstones and sandstones with anhydrite interbeds to dolomites to anhydrites with clayey silt interbeds.

	GWB	ERDA-6
Borate	158 mM	63 mM
Na^{+}	3.53 M	4.87 M
Mg^{2+}	1.02 M	19 mM
K^{+}	0.467 M	97 mM
Ca^{2+}	14 mM	12 mM
SO_4^{2-}	177 mM	170 mM
Cl^{-}	5.6 M	4.8 M
Br^{-}	26.6 mM	11 mM
HCO_3^{-}	Not reported	16 mM
pH	Not reported	6.17
Ionic Strength (M)	7.44	5.32

Table 2-1. WIPP representative brine compositions (from DOE 2014c)

2.3 Overyling Formations

Overlying the Rustler are the Triassic Dewey Lake Formation and Santa Rosa, followed by the Cenozoic Ogallala, Gatuna, and Quaternary deposits. These formations are composed of

sedimentary rocks, including iron-rich sandstones and siltstones, conglomerates, caliche, and surficial sediments, such as sand dunes.

2.4 Underlying Formations

Underlying the WIPP is the Delaware Mountain Group, composed of the Bell Canyon, Cherry Canyon, and Brushy Canyon Formations. Beneath 2,600 meters are lower Permian units, such as the Wolfcamp and the Bone Spring Formations. Both of these lower units are a series of shales, carbonates, and sandstones that are significant because they contain abundant oil and natural gas. Because of the advent of drilling techniques, including horizontal drilling and hydraulic fracturing, these "unconventional" formations have received renewed attention and have been drilled extensively in recent years. Drilling activity is one of the biggest risks for a release of nuclear waste material at WIPP if oil and gas drilling accidentally penetrates the repository.

Karst

Karst systems, or the topography and processes associated with the formation of caves and sinkholes, have been an ongoing concern for WIPP stakeholders. The Rustler Formation, which contains the Culebra and Magenta Dolomites, appears to thin westward of the repository toward an area referred to as Nash Draw. Nash Draw represents a topographical low in the region where infiltration of water into the system results in dissolution of the Rustler, creating sinkholes. Local topographic depressions near the WIPP site and a lack of surface runoff at the WIPP also contribute to the perception that karst could be occurring close to the repository. A nearby—although unrelated—feature that has drawn attention to karst is Carlsbad Caverns, which is formed within the Capitan Reef, a massive carbonate.

Multiple studies have assessed the potential for karst formation at the WIPP site and have concluded that it would be unlikely (e.g., Lorenz 2006a and 2006b). For karst formation to occur, reactive water, such as precipitation, would have to infiltrate into the Culebra dolomite, resulting in the dissolution of the underlying evaporite minerals. Combined with the very low precipitation in the region, as well as evapotranspiration of the overlying flora, very little water (if any) is likely to infiltrate deeper than 200 meters into the Culebra. Additionally, the dolomite is not hydrologically connected to the units below, which means meteoric water will not infiltrate into the underlying evaporites.

Box 2-1. Karst

2.5 Properties of Rock Salt

The thick evaporite deposits at the WIPP were chosen for nuclear waste disposal because of the ductile properties of halite, or rock salt. When stresses are applied to the mineral, the crystallographic structure of halite plastically deforms. On large scales, this results in the ability for salt to "creep" and encapsulate the waste, thereby sealing it away from the rest of the environment. Its ductile behavior over geologic time and its self-sealing abilities mean that salt beds have extremely low porosity ($\ll 1\%$) and are essentially impermeable, preventing any groundwater infiltration from entering the repository and mobilizing waste. These bedded salt deposits also occur in an area with little groundwater and in a tectonically stable region. Although the rock salt is very ductile, the Salado is not entirely composed of pure halite and has anhydrite and clay interbeds. These impurities make parts of the Salado more brittle and allow the formation and preservation of isolated fractured layers that can contain pressurized brine.

2.6 WIPP Geochemistry

If the repository is left undisturbed, PA calculations show that waste stored within the WIPP should remain intact and that releases into the accessible environment are expected to be negligible because of the low permeability of the Salado, as well as its isolation from the overlying rock units (Section 9.1).

That is, the radionuclides won't migrate out of the waste area because of the favorable conditions in the disposal system. However, because the underlying Bell Canyon Formation hosts an abundance of oil and gas reserves, the WIPP PA includes an assessment of potential releases from accidental drilling that can bring waste to the surface and/or intersect an underlying brine pocket that then interacts with the waste. For example, gas pressures resulting from corrosion and radiolysis (see Sections 6.2.2 and 6.3.1) will affect spallings (solid material carried into the borehole due to pressure release—see Section 10.2.2). Oil and gas drilling also may cause a low-probability accidental brine release. The geochemical interactions building up to a brine release are described below. The proceeding sections provide the underlying concepts behind the various interactions.

2.6.1 WIPP Chemical Conditions

On closure of the WIPP, repository pressures will begin to increase—in part because of pressures created by creep closure, as well as through gas generation reactions and the possible inflow from the Castile into the repository. The maximum post-closure repository pressures will approximate lithostatic pressures, at approximately 150 atm (15 MegaPascals or 15 MPa). The minimum pressure needed for a release of brine to the surface as a result of a drilling intrusion is approximately 80 atm (8 MPa). The composition of the brine will be a result of multiple repository processes described below.

Because of high thermal conductivity from the surrounding halite, repository temperatures will remain at approximately 27ºC and likely stay close to that temperature, although heat generated from the waste may increase temperatures by up to 12ºC (DOE 2019d). Although the WIPP is situated in a formation that allows little water infiltration, the Salado contains intragranular and intergranular brine, allowing brine seepage into the repository to occur. The clay zones and anhydrites may also contribute limited brine seepage. Brine may infiltrate during the repository's post-closure history and interact with the actinides and waste contents in the repository. When water infiltrates the waste area, a variety of reactions will occur that will influence the potential for radionuclides to be released.

After the repository is closed, brine seepage may occur, resulting in humid conditions that will be conducive to CPR degradation. Microorganisms living in the brine, on the salt, and in the wastes will feed off the carbon from the CPR to produce hydrogen sulfide (H_2S) and carbon dioxide (CO_2) gases. Brine also will interact with the iron and lead in the waste canisters to produce hydrogen (H_2). These reactions will also consume oxygen (O_2), making the environment anoxic. Much of the H_2S gas will interact with waste canisters and precipitate as solid iron sulfide (FeS), whereas most of the CO_2 will be consumed by the emplaced MgO. Additional gas generation will occur as water is split by radiolysis caused by the alpha decay of the actinides in the waste, also producing H_2. Because of the removal of all other gases through multiple reactions, the gas phase in the repository will consist largely of H_2. The activity of these gases will only be exacerbated by the increase in pressure as the Salado halite begins to creep close and encapsulate the waste and if pressurized brine enters the repository. Combined with the anoxic iron corrosion, the repository will exhibit reducing conditions.

At the same time, brine also will dissolve and equilibrate with components in the waste, as well as with the actinides. Brine will interact with the cementitious material ($Ca(OH)_2$) and precipitate carbonates ($CaCO_3$). The MgO backfill will hydrate to form brucite ($Mg(OH)_2(s)$), which will remove CO_2 produced from the microbial activity discussed above. Both reactions are designed to buffer repository pH and keep conditions close to pH values of 8 to 10.

Actinides, meanwhile—including Np, Pu, thorium (Th), U, Am, and Cm—will interact with ions in the WIPP brines, organics in the WIPP waste stream, and themselves, forming ions and aqueous complexes. The solubility of these actinides will be affected by the reducing conditions created by the existence of pressure, H_2, H_2S, and the electron transfer resulting from microbial activity and anoxic steel corrosion. These reducing conditions result in conditions that extend the range at which certain actinides with lower

valence states can be stable. Consequently, actinides with reduced valence states, such as Pu^{3+}, likely will be the dominant source term (i.e., the dissolved actinide released into the surrounding environment).

Dissolved actinides in the brine can react with one another to form actinide macromolecules (mineral fragment and intrinsic colloids). Actinides may also interact with larger components in the solution, including humic substances, microorganisms, and mineral fragments, to form macromolecules. Complexation or sorption of these actinides will result in further colloid formation that will increase the potential amount of actinide released into the environment.

WIPP calculations also consider possible brine flow to the Culebra, the most transmissive member of the Rustler Formation, which would lead to actinide migration to the Land Withdrawal Boundary. Estimating migration through the Culebra requires understanding the extent of sorption and removal that can occur between the source term and surrounding host rock.

3 Solution Chemistry

The experiments and models used to understand WIPP geochemistry are built on some fundamental principles of aqueous geochemistry. Much of the WIPP geochemistry focuses on how solids interact with the surrounding water, and this section outlines concepts used to understand this interaction, including units of measure and equilibrium. This unit also describes how geochemists consider salinity and ionic interactions in solutions, which is extremely important in the hypersaline brines present in the repository.

In the following section, we will describe various solution chemistry principles using the example from Figure 3-1 below. When a solid Np(V) species, $NpO_2OH(s)$, is placed in a beaker of deionized water with no contact to any gases, we see the dissolution of the mineral, resulting in the mobilization of Np(V) ions in the form of NpO_2^+. This dissolution can be expressed in the following equation:

$$NpO_2OH(s) + H^+ \rightleftharpoons NpO_2^+ + H_2O \quad \text{Equation 3-1}$$

Besides Np dissolution, water will also have reactions involving the dissociation of water into proton (H^+) and hydroxide (OH^-):

$$H_2O \rightleftharpoons H^+ + OH^- \quad \text{Equation 3-2}$$

NpO_2^+ also will react with the water and form $NpO_2OH(aq^*)$ and $NpO_2(OH)_2^-$ (discussed in Section 5.2).

Adding ionic compounds, such as NaCl, introduces additional reactions to the system. The Np(V) solid could react with any of the added ions, introducing new interactions and calculations to consider, as illustrated in Figure 3-1.

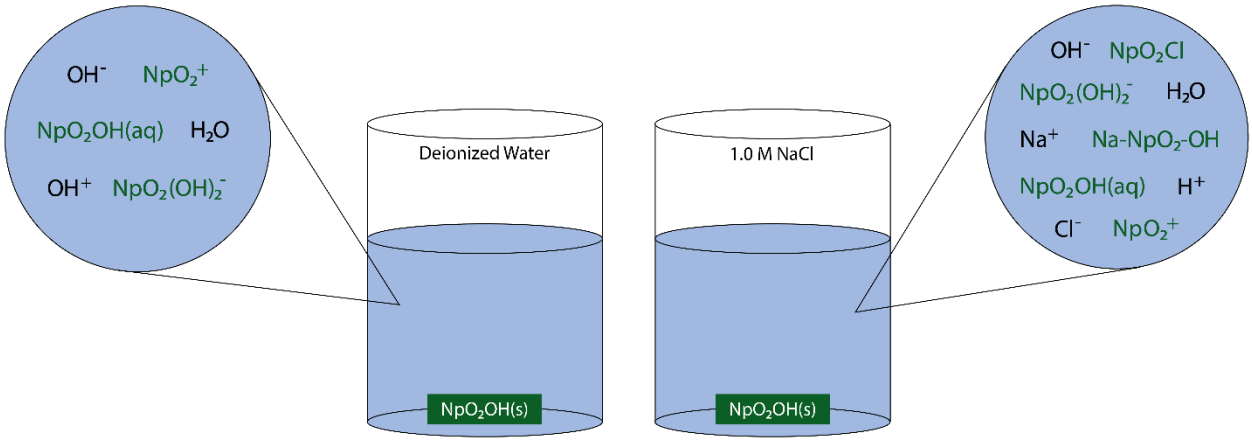

Figure 3-1. Example of Np(V) solid dissolution in deionized water and in 1.0 M NaCl

3.1 Units

Solutes, or the dissolved organic and inorganic constituents in a solution, are most commonly reported in milligrams per liter (mg/L) or parts per million (i.e., mg per kilogram), such as that written in the WIPP's site environmental reports (DOE 2017a and 2017b). However, in describing chemical reactions, the most useful units of measurements are *molar* and *molal* quantities. Molar refers to the number of moles of a constituent per liter (mol/L or M) of solution, whereas molal refers to moles per kilogram (mol/kg or *m*) of water. For example, chemical reactions and thermodynamic calculations commonly are calculated

[*] All species are aqueous (aq) unless they have been designated otherwise.

using molar quantities, and solubility calculations using representative WIPP brines (Table 2-1) are performed using molal or molar units.

3.2 Ionic Strength

The ionic strength of a solution is the concentration (mol/L or mol/kg water) of all ions present in that solution, calculated as one-half the sum of all the ions present in a solution multiplied by the square of the ion's charge:

$$I = \frac{1}{2}\sum c_i(z_i)^2 \quad \text{Equation 3-3}$$

where c_i is the concentration of the ion (M), and z_i is its charge. Because no ions are in the first beaker from Figure 3-1, the ionic strength of the solution without any Np(V) is close to 0. Given the charge of Na^+ is +1 and Cl^- is −1, the ionic strength of the 1.0 M NaCl solution is 1.0 M (½ × $(+1^2 + -1^2)$ = 1.0).

Ionic strength is important because more ions in solution mean more complicated reactions from increased ion-ion interactions. The ionic strength of rainwater is generally close to 0.002 M. Groundwater can have ionic strength ranging between 0.001 and 0.2 M. Seawater has an ionic strength of approximately 0.7 M (e.g., Appello and Postma 2004). In contrast to all of these, the brines sampled from the WIPP have ionic strength ranges between 5.32 and 7.44 M (DOE 2014c).

3.3 Activity

The ions and complexes in a solution are charged species that interact with each other, affecting each other's behavior and that of the solution itself. Because of this, geochemists perform calculations using the activity of these constituents, rather than their concentrations. The activity of a constituent in a solution refers to its *effective concentration*, which is an adjusted concentration to account for the interactions of constituents in a solution with each other and the solvent (e.g., water). Concentration is adjusted to become activity by multiplying the concentration of a constituent with an activity coefficient, γ_i. This relationship can be represented by the following equation:

$$a_i = \gamma_i c_i \quad \text{Equation 3-4}$$

where c_i is the concentration of the constituent, and a_i is its activity.

The activity of the NpO_2^+ ions in the distilled water of Figure 3-1 will differ from the activity of those same ions in the 1.0 M NaCl because of the increased ionic strength and ion interactions of the second solution. This change in activity also will change the effective concentration of the dissolved NpO_2^+, altering the degree of Np(V)

Calculating Activity

For solutions with low ionic strengths, the Debye-Hückel approach can be used to estimate activity coefficients:

$$log\gamma_i = -Az_i^2\sqrt{I}$$

where A is a constant, I is ionic strength, z_i is an ion's charge, and γ_i is the activity coefficient.

As ionic strength increases, the Davies approach can be utilized:

$$\log\gamma_i = -Az_i^2\left(\frac{\sqrt{I}}{1+\sqrt{I}}\right) - 0.3I$$

For even more accurate activity coefficient calculations, the specific ion interaction theory approach can be used (e.g., Grenthe et al. 2013). This approach uses a *virial expansion* equation, which begins with the Debye-Hückel approach (D) for a specific ion (j) and adds further equations representing that ion's interactions with other ions (k) and their molalities (m_k) in a solution of a specific ionic strength I_m. These interactions can be determined using empirical data. This approach is generally usable up to ionic strengths of 3 M.

$$\log\gamma_j = -z_j^2 D + \sum_k \varepsilon(j,k,I_m)m_k$$

Box 3-1. Calculating activity

dissolution that will occur, as well as the various forms of Np(V) we will expect to find in solution.

Activity coefficients are estimated by accounting for different factors that may affect ions in a solution, such as ionic strength, ion-ion interactions due to ion size, electrostatic interactions, and charge. Some approaches include using the Debye-Hückel or Davies methods to calculate the activity coefficient at low ionic strengths. See Box 3-1 for more information.

3.3.1 Activity Coefficients and WIPP: The Pitzer Approach

Although many activity coefficients can be estimated using the Debye-Hückel, Davies, or specific ion interaction theory (SIT) approaches, these equations usually only approximate coefficients for dilute solutions. For ionic strengths greater than 3 M, such as those relevant to conditions found in the WIPP, other approaches are needed to estimate activity coefficients and more accurately calculate activity. This, in turn, leads to more accurate geochemical predictions.

Pitzer and coworkers have calculated activity coefficients by using the Debye-Hückel approach and using a virial expansion equation, in which different terms are added after the Debye-Hückel equation to account for different aspects of ion-ion interactions. This approach is semi-empirical, because the terms added to the equation are experimentally derived and calculated. The WIPP PA uses the Pitzer approach to determine ion activity. Because many of the parameters in this equation are experimentally derived, data collection efforts are ongoing, resulting in incomplete datasets, potentially propagating uncertainty into geochemical models.

3.3.2 pH, p_cH, and p_mH

The pH of a solution is a measure of the solution's hydrogen ion *activity* (a_H), expressed as a negative logarithm:

The Pitzer Equations

Ion activity coefficients in high-ionic-strength solutions can be calculated using Pitzer equations, a virial expansion equation in which different terms are successively added onto an equation to represent different nuances in ion-ion interactions. The equation is filled with multiple parameters, more so than SIT equations. Many of these parameters sum up the concentration of different ions, charges, and ion-ion interactions. Below is an example of the Pitzer virial expansion equation used to calculate an activity coefficient (γ_i) (e.g., Felmy and Weare 1986).

$$\ln \gamma_i = \ln \gamma_{DH} + \sum_j B_{ij}(I) m_j + \sum_{jk} C_{ijk}(I) m_j m_k + \cdots$$

New terms can be added to this equation depending on the system being described. In this equation, i, j and k refer to the various ions present in the solution, and m refers to the molal concentrations of these ions in solution.

The first term ($\ln \gamma_{DH}$) relates to the Debye-Hückel equation that is used to calculate activity coefficients at low ionic strength (see Box 3-1). Terms added beyond the Debye-Hückel are ion-ion interaction parameters that are experimentally derived. The B term is calculated using β(0), β(1), β(2), α(1), α(2), all of which can be calculated experimentally. Similarly, the C term is calculated using the C(ϕ) and other terms. The β, α, and C(ϕ) can be found in the WIPP actinide database used for geochemical modeling. As part of its review of the WIPP's PA, EPA evaluates DOE's use of Pitzer coefficients and how they were experimentally derived.

Box 3-2. The Pitzer equations

$$pH = -loga_{H^+}$$ Equation 3-5

The scale of pH in natural waters typically falls between 0 and 14 and describes how acidic or how basic a solution is. Because this is expressed as a negative logarithm, low pH values represent solutions with a high H^+ activity (i.e., acidic solutions), whereas solutions with a high pH represent solutions with a low H^+ activity (i.e., basic solutions). Solutions with a high pH also will have a higher OH^- activity. Equation 3-2 also describes the relationship between H^+ and OH^-. In this equation, the product of the activities of both H^+ and OH^- reach a constant value (K_w, discussed further in Section 3.4.1).

Reactions at Equilibrium

Actinide solubility reactions in WIPP brines are assumed to be in equilibrium in the PA, and the amount of time it takes for a reaction to be at equilibrium can vary depending on the reaction. Many other reactions, although not at equilibrium, are modeled using equilibrium constants, meaning their values may be derived from experiments that were at equilibrium. The amount of time at which a reaction can reach equilibrium may vary, ranging from minutes, such as with aqueous carbonate reactions, to thousands of years, such as with precipitation of some silicates.

One important reaction in the WIPP is the dissolution of hydromagnesite. Hydromagnesite itself is a metastable mineral (i.e., the solid is thermodynamically unstable), but because it persists over geologic time, it is treated as if it were stable for the purposes of modeling. This reaction is one in a series of reactions related to the MgO engineered barrier used to control CO_2 in the repository (which will affect pH and actinide complexation; see Section 4.3.3.2).

$$Mg_5(CO_3)_4(OH)_2{\bullet}4H_2O\ (s) \rightleftharpoons 4CO_3^{2-} + 5Mg^{2+} + 2OH^- + 4H_2O$$

Deriving a solubility constant requires that the mineral dissolution reaction be at equilibrium. During hydromagnesite's dissolution—shown in the figure below, adapted from Gautier et al. (2014)—Mg^{2+} is released. Mg^{2+} enters solution at different rates during the course of the reaction, and when the Mg^{2+} release reaches a steady state, we assume equilibrium has been achieved because these are the concentrations at which the solution has been saturated with Mg^{2+}. Part of EPA's review of DOE-derived equilibrium constants is to ensure that log K values are derived under conditions of equilibrium so that estimates of solubility and the extent to which this mineral can buffer CO_2 are accurate.

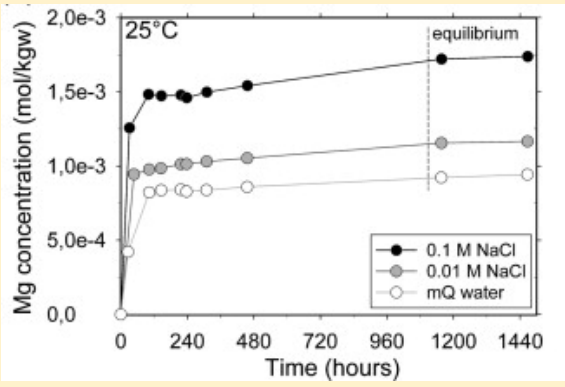

Box 3-3. Reactions at equilibrium

$$K_w = a_{H^+} \times a_{OH^-} = 10^{-14} \quad \text{Equation 3-6}$$

In acidic solutions (i.e., high H^+ activities), OH^- activities are lower, and in basic solutions, the opposite occurs. At neutral pH values, $a_{H+} = a_{OH-} = 10^{-7}$.

The pH of a solution is measured using a pH electrode, which measures the electrical potential between a defined solution and an unknown solution separated by a glass membrane. Because of this, pH electrodes measure pH as the activity of H^+ ions and not the concentration. In dilute solutions, the measured pH approximately reflects the concentration of H^+ in the solution. However, in solutions with higher ionic strength, such as in Figure 3-1 or WIPP brine, pH electrodes are less accurate because of inaccuracies measuring the potential between the electrode's defined solution and the brine. In the case of WIPP brine, a correction factor is added to measured pH. This corrected pH is referred to as p_cH, which represents the negative logarithm of the hydrogen ion *concentration* (in M) rather than activity. This variable is calculated with the following equation (e.g., Roselle 2011) and can be determined by measuring pH in a dilute solution and calculating the difference in pH as it changes in a series of solutions of increasing ionic strength:

$$pcH = pH + A \quad \text{Equation 3-7}$$

where A represents the correction factor. The difference between pH and p_cH in WIPP brine can be significant. For example, the pH for ERDA-6 brine in the 2019-CRA was calculated as 8.82. However, when adjusted for p_cH, the value increases to 9.52 (Domski and Sisk-Scott 2019). Alternatively, pH can be adjusted to p_mH, which refers to the negative logarithm of hydrogen ion concentration in molal units.

The pH, p_cH, and p_mH of solutions are critical geochemical variables that influence multiple geochemical processes, including the degree of mineral dissolution that can occur, the speciation of different aqueous complexes, the amount of gas that can dissolve in solution, the transfer of electrons between different aqueous species, and the degree of sorption that may occur for ions interacting with a solid phase. An accurate accounting of H^+ activity and concentration in solution can make a big difference in modeling the extent of an actinide release.

For example, Equation 3-1 shows that Np(V) dissolution occurs when H^+ interacts with $NpO_2OH(s)$. The amount of H^+ present in the solution will affect the quantity of the NpO_2^+ that will be mobilized. As pH increases, the NpO_2^+ concentrations will decrease. At very high pH, dissolved Np(V) concentrations begin to increase again, because of hydrolysis, where the dissolved metal begins to complex with water molecules (Section 5.2). This means that Np(V) solubility is at its lowest at a narrow pH range. Most actinides follow a similar dissolution pattern, making pH control vital to the WIPP's performance as a repository. These interactions will be explored further in Section 4.

A number of processes at the WIPP may affect pH. Such processes as microbial respiration could generate CO_2 and decrease pH by generating carbonic acid (see Section 4.3). On the other hand, waste inventory items, such as cements (e.g., $Ca(OH)_2(s)$), could increase the pH by adding OH^- into the system. The MgO engineered barrier included in the waste inventory is one such aspect that ensures pH is adequately buffered so that actinide solubility can stay at a minimum in the event of a brine release (Section 4.3.3.2).

3.4 Equilibrium

WIPP geochemical models assume that geochemical reactions are at equilibrium, which occurs when the activities of the products and reactants reach a constant value and when the total free energy of a system is at a minimum. Note that not all reactions and species at the WIPP are assumed at equilibrium—such as anoxic corrosion, redox, or the persistence of such amorphous or metastable solid phases as

hydromagnesite—although the values used to model all these reactions are derived from experiments that were at equilibrium. Reactions in disequilibrium can be modeled by adjusting model input parameters.

3.4.1 Equilibrium Constants

Chemical reactions usually come in the following form:

$$aA + bB \rightleftharpoons cC + dD$$

$$\text{reactants} \rightleftharpoons \text{products}$$

where the lowercase letters (a, b, c, d) represent the stoichiometric (molar or molal) quantities of each chemical constituent (A, B, C, D) in the reaction. For this example, the equilibrium constant is calculated through the following equation:

$$K = \frac{a_C^c \, a_D^d}{a_A^a \, a_B^b} \quad \text{Equation 3-8}$$

where *a* represent the *activity* of each constituent present. K values tend to be expressed as exponents with non-whole numbers to make the interchange between logarithmic and non-logarithmic scales easy. These values also allow us to calculate the concentrations of each ion needed to reach equilibrium.

Equilibrium constants can be used for such reactions as the dissociation of water (Equation 3-2):

$$H_2O \rightleftharpoons H^+ + OH^- \text{ where } K_w = a_{H^+} \times a_{OH^-}$$

Note that in this equation, H_2O has been removed from the denominator. Usually, both water and solids are assigned an activity of 1, which means they do not need to be included in the equation. However, as solutions become more saline, the increased ionic strength will begin to affect water's behavior, and its activity will be important in calculating equilibrium constants.

3.4.2 Equilibrium Constants and the WIPP

Below are a few examples of reactions that are important to the WIPP, as well as their equilibrium constants. Each of these topics will be discussed later in this document.

- *Dissolution/Precipitation:* Dissolution of $CaSO_4$ contributes to the salinity of WIPP brine. Note that K_{sp} is an equilibrium constant that is referred to as a solubility product for mineral dissolution (e.g., Stumm and Morgan 1996). Also note that $CaSO_4$ is excluded from the equation because solid phases are given unit activity in calculating equilibrium constants.

$$CaSO_4(s) \rightleftharpoons Ca^{2+} + SO_4^{2-} \quad \text{Equation 3-9}$$

$$K_{sp} = a_{Ca^{2+}} \times a_{SO_4^{2-}} = 10^{-4.36}$$

- *Gas Chemistry:* The dissolution of CO_2 gas has important pH implications and is controlled through the MgO engineered barrier. In this case, K_H is the equilibrium constant for gas dissolution, also known as the Henry's Law constant. Furthermore, fCO_2 refers to the gas's fugacity, a concept that is analogous to activity (e.g., Appelo and Postma 2005). A gas's fugacity relates to its *effective* partial pressure rather than the partial pressure of the gas itself:

$$CO_2(g) + H_2O(l) \rightleftharpoons H_2CO_3 \quad \text{Equation 3-10}$$

$$K_H = \frac{a_{H_2CO_3}}{f_{CO_2}} = 10^{-1.5}$$

- *Complexation:* Ions will complex with other ions and with water, having implications toward total actinide concentrations and mobility. K values for complexation reactions often are given the term β because they describe an association of two ions instead of dissolution. Although Th is not a transuranic element, it is present in the WIPP waste and used widely as an analog to calculate the solubility of +IV actinides. An example of Th complexation reactions is presented below:

$$Th^{4+} + 4OH^- \rightleftharpoons Th(OH)_4(aq) \quad \text{Equation 3-11}$$

$$\beta = \frac{a_{Th(OH)_4}}{a_{Th^{4+}} \times a_{OH^-}^4} = 10^{38.5}$$

- *Redox:* Oxidation/reduction (redox) reactions describe the movement of electrons (e^-) in a solution. Redox reactions affect repository gas chemistry, corrosion, and actinide solubility (e.g., Lemire et al. 2013):

$$Fe(cr) \rightleftharpoons Fe^{2+} + 2e^- \quad \text{Equation 3-12}$$

$$K = a_{Fe^{2+}} \times a_{e^-}^2 = 10^{0.16}$$

The Thermodynamics of Equilibrium

In aqueous geochemistry, systems often are assumed to be in chemical equilibrium, even though they are rarely so in reality. Equilibrium provides a useful approximation to the real world and can indicate the direction a chemical reaction is going. Systems in equilibrium refer to a state of minimum energy, which is represented through a change in the Gibbs free energy of a reaction, ΔG_R. When a system is in equilibrium, $\Delta G_R = 0$. This is measured in kilojoules per mole (kJ/mol).

Related to ΔG_R is ΔG^o_R or the standard Gibbs free energy of the reaction. This value relates ΔG_R to chemical potential, the form of energy that can be absorbed or released in a reaction. Other terms associated with ΔG^o_R include μ^o and μ^o_i.

Both forms of ΔG are related to equilibrium through the following equation:

$$\Delta G_R = \Delta G_R^0 + RTlnK$$

where R is the gas constant (8.314×10^{-3} kJ/mol/deg), T is temperature in Kelvin, and lnK is the natural log of the equilibrium constant of a chemical reaction. Note that temperature is included in this equation, which means that the equilibrium constants also depend on temperature. When the system is in equilibrium, the equation can be rearranged so that ΔG_R is removed because at equilibrium, $\Delta G_R = 0$:

$$\Delta G_R^0 = -RTlnK$$

ΔG^o_R is further related to the Gibbs free energy of formation, ΔG^o_f. This constant describes the energy needed to produce one mole of a substance from pure elements in their most stable form. In a chemical equation, each reactant and each product has a value for ΔG^o_f, which can be experimentally derived. ΔG^o_f can then be related to ΔG^o_R when the formations of the reactants and products are tabulated, that is:

$$\Delta G_R^0 = \sum \Delta G_{f\ products}^0 - \sum \Delta G_{f\ reactants}^0$$

Equilibrium constants can be calculated if the formation constants are known, often found in various lookup tables (e.g., Hummel et al. 2005). These values, including free energy and chemical potentials, are determined at standard conditions (i.e., 1 bar pressure and 273.15K). Values for K and log K at the WIPP are calculated using these constants, and various organizations—such as the the Organisation for Economic Co-operation and Development (OECD) Nuclear Energy Agency (NEA)—compile these values from the literature for public use.

Box 3-4. The thermodynamics of equilibrium

4 Mineral Precipitation and Dissolution

Precipitation and dissolution reactions result from the interactions between minerals and groundwater and involve the transfer of mass to and from the aqueous phase. These reactions control multiple aspects of the WIPP, ranging from the composition of GWB and ERDA brines to reactions with the MgO engineered barrier to the corrosion of the waste containers to the concentrations of actinides that may be present in a release. This section describes dissolution, precipitation, and the factors that can influence these reactions, such as pH, activity, temperature, and mineral crystal structure.

4.1 Dissolution

4.1.1 Solubility Product

Many dissolution reactions may simply reflect the dissociation of two ions from a solid, such as with NaCl or with $CaSO_4$ (Equation 3-9), shown below:

$$NaCl(s) \rightleftharpoons Na^+ + Cl^- \quad \text{Equation 4-1}$$
$$CaSO_4(s) \rightleftharpoons Ca^{2+} + SO4_2^- \quad \text{Equation 3-9}$$

These two minerals compose the bulk of the Salado, and the ions from these dissociation reactions are key constituents of the WIPP brine. Mineral precipitation and dissolution reactions are represented using the solubility product K_{sp}, which is the equilibrium constant that describes when the mineral dissolves in pure water to its constituent ions. As with the other reactions previously described, K_{sp} is calculated using ion activity. The solubility products for both halite and anhydrite are shown below:

$$K_{sp,halite} = a_{Na^+} \times a_{Cl^-} = 10^{1.57} \quad \text{Equation 4-2}$$
$$K_{sp,anhydrite} = a_{Ca^{2+}} \times a_{SO_4^{2-}} = 10^{-4.36} \quad \text{Equation 3-9}$$

Solids are considered to be at unit activity (i.e., activity = 1) and therefore are not considered in the calculation of K_{sp}.

4.1.2 Relationship to pH

Other minerals, such as $CaCO_3$, also can be represented through similar dissociation reactions:

$$CaCO_3\ (s) \rightleftharpoons Ca^{2+} + CO_3^{2-} \quad \text{Equation 4-3}$$

However, carbonate speciation in a solution is complex, involving multiple steps, and is heavily pH dependent (discussed later in this section), with particular carbonate species predominating depending on the pH of the solution. As a result, this same reaction could be written in multiple ways:

$$CaCO_3(s) + 2H^+ \rightleftharpoons Ca^{2+} + H_2CO_3 \quad \text{Equation 4-4}$$
$$CaCO_3(s) + H^+ \rightleftharpoons Ca^{2+} + HCO_3^- \quad \text{Equation 4-5}$$

Note the addition of H^+ in the reactions, showing that the dissolution of carbonate minerals occurs when calcite removes H^+ from solution. Many other mineral dissolution reactions also can be affected by pH, including many WIPP-relevant phases, such as borax ($Na_2B_4O_7 \cdot 10H_2O$), brucite ($Mg(OH)_2$), hydromagnesite ($Mg_5(CO_3)_4(OH)_2 \cdot 4H_2O$), steel minerals, and actinide-bearing solids.

Most metals and actinides are highly soluble at both low and high pH values. If we consider the example of NpO_2OH(s) from Figure 3-1, its dissolution occurs when the solid interacts with a proton:

$$NpO_2OH(s) + H^+ \rightleftharpoons NpO_2^+ + H_2O \quad \text{Equation 3-1}$$

Actinides and metals released into the aqueous phase also will complex with water and other ions in the solution. As a result, the total concentration of Np in the solution will be the sum of Np^{5+} (which is NpO_2^+), as well as the multiple complexes it creates:

$$[Np]_{total} = [NpO_2^+] + [NpO_2OH] + [NpO_2(OH)^{2-}] + \ldots$$

Figure 4-1 shows that total dissolved Np increases at high and low pH. There is a specific pH range, in this case approximately 10.5–13.5, where Np solubility remains at a minimum. Because other actinides follow similar dissolution patterns, buffering WIPP brine pH to a range where dissolution is at a minimum remains vitally important.

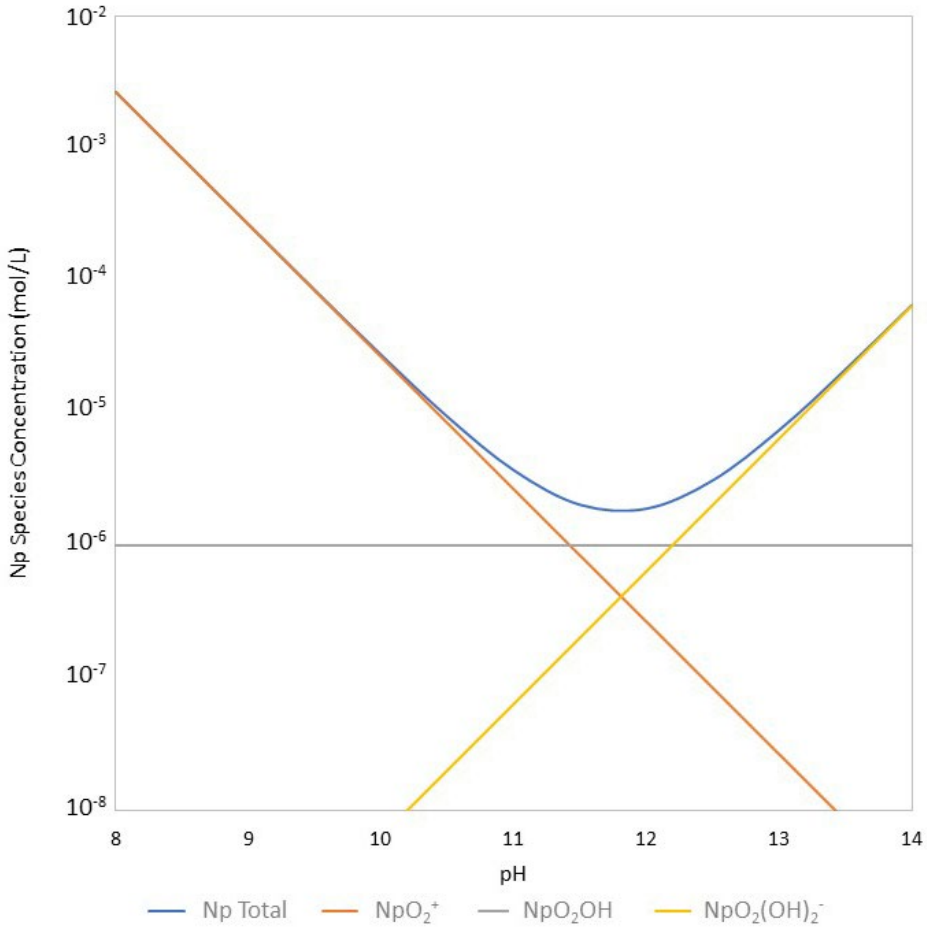

Figure 4-1. $NpO_2OH(s)$ solubility in 0.1 M NaCl

4.1.3 Relationship to Activity

Because of the few ion interactions in dilute solutions, ion activity and ion concentration are approximately equal. However, in solutions of high ionic strength, such as with the WIPP, ion activities can differ drastically from ion concentrations (see Section 3.3). Consequently, the salinity of a solution can affect how much a mineral will dissolve. For example, $NpO_2OH(s)$ will dissolve into different quantities at changing ionic strengths. In this case, the increased ionic strength results in more dissolved $NpO_2OH(s)$; however, this can vary, depending on the ions and the system being examined (Figure 4-2).

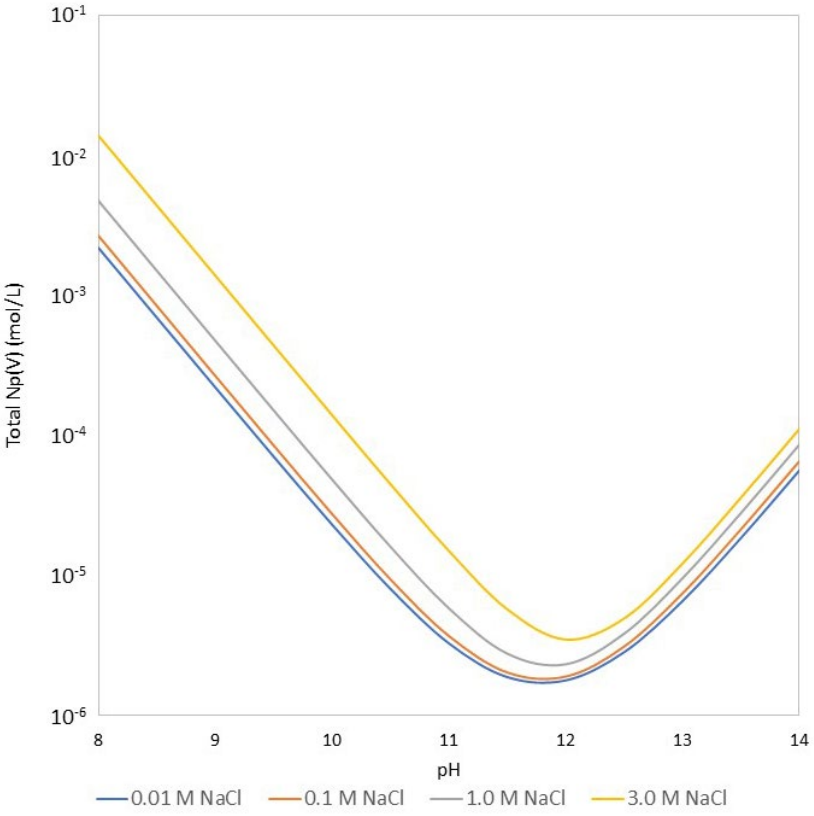

Figure 4-2. Ionic strength effects on $NpO_2OH(s)$ dissolution

Saturation Index

Saturation index (SI) is a useful way to understand how minerals are interacting with groundwater and whether reactions favor mineral dissolution or precipitation. Solubility product (K_{sp}) is calculated according to Equation 3-9 using the activities of the ions in solution. This same formula also is used to determine the ion activity product (Q), which can then be used to compare to K_{sp} and to calculate SI. When $Q = K_{sp}$, the solution is in equilibrium. From this, we can compare Q to K and determine how close or how far from equilibrium a solution may be:

$$\mathrm{SI} = \log \frac{Q}{K}$$

When Q < K, SI values are negative, and a solution is undersaturated with respect to a mineral. At equilibrium, Q = K and SI values are at 0. When Q > K, SI values are positive, and the solution is supersaturated with respect to the mineral.

Box 4-1. Saturation index

4.1.4 Relationship to Temperature

Box 3-4 in Section 3.4 shows that in determining thermodynamic equilibrium, temperature is involved in the calculation of free energy and of equilibrium constants. This, in turn, shows that temperature will have an effect on precipitation and dissolution reactions. In the WIPP, temperature conditions throughout the life of the repository are expected to be around 27ºC without major fluctuations. As a result, the effects of temperature on solubility effectively can be ignored for the system.

4.2 Precipitation

Equilibrium refers to the state when the activity of the products and reactants reach a constant value. When the concentration of the products is below this constant value, solutions are undersaturated with respect to a mineral being examined, and dissolution tends to occur. When the concentration of the reactants is above the constant value, the solution is considered supersaturated with respect to that same mineral and conditions favor mineral precipitation (see Box 4-1 for more details).

4.2.1 Precipitation Reactions

The interaction of chemical constituents in the repository can result in the precipitation of insoluble minerals. When zero-valent iron, or steel (Fe^0(cr)), for example, reacts with sulfide produced during microbial CPR degradation, a new solid, FeS, can precipitate:

$$Fe^0(cr) + H_2S(g) \rightleftharpoons FeS(s) + H_2(g),\ K_{sp} = 10^{0.012} \quad \text{Equation 4-6}$$

Such corrosion reactions alter the composition of the repository gas phase by potentially removing biologically produced sulfide and replacing it with hydrogen gas. This has implications for the redox of the repository discussed later in this document.

Another important precipitation reaction involves the interaction of cement from the waste with the brine. Cement can be represented by its reactive component, such as the mineral $Ca(OH)_2$, and its dissolution or precipitation affects the release of both Ca^{2+} and OH^- ions. The excess of Ca^{2+} added into a system from $Ca(OH)_2$ can interact with CO_2 in the system, resulting in calcite precipitation. The release of OH^- can increase the pH of the system, which, in turn, can increase actinide solubility.

$$Ca(OH)_2(s) \rightleftharpoons Ca^{2+} + 2OH^- \quad \text{Equation 4-7}$$

However, components in the brine, such as the $MgCl_2$(aq) complex, will react with the cement, resulting in the precipitation of $Mg(OH)_2$ and no pH increase.

$$Ca(OH)_2(s) + MgCl_2(aq) \rightleftharpoons CaCl_2(aq) + Mg(OH)_2(s) \quad \text{Equation 4-8}$$

$Mg(OH)_2$ also is important to control CO_2 within the repository (Section 4.3.3.2). Because cement can have major effects on repository pH, the WIPP monitors the inventory of cement entering the repository to ensure that the Ca^{2+} inventory from cement does not exceed the amount of Mg^{2+} in brine available to react.

4.2.2 Amorphous and Crystalline Minerals

Different crystal structures of the same mineral can exist (i.e., polymorphs) despite being composed of the same chemical formula. This makes selection of an equilibrium constant for a precipitate difficult. $CaCO_3$, a common example, can be multiple different minerals, including calcite, aragonite, and vaterite. These minerals all have varying forms of crystallinity resulting from aging processes, and thus have different K_{sp} values. This difference in K_{sp} also will dictate the magnitude of dissolution and precipitation that may occur. Minerals may take on hydrous forms as well. For $CaCO_3$, this could be such forms as $CaCO_3.6H_2O$ or $CaCO_3.H_2O$ (ikaite and monohydrocalcite, respectively), which can occur as the carbonate mineral precipitates and begins to age and change in crystal structure.

Actinide minerals also will have different crystallinities, and the choice of which mineral to represent in the PA will affect the degree of a release. For example, the Am solid phase expected at the WIPP, $Am(OH)_3$, can either be amorphous (am) or crystalline (cr) and will dissolve to release the highly soluble Am^{3+}.

$$Am(OH)_3(am) + 3H^+ \rightleftharpoons 3H_2O + Am^{3+}, K_{sp} = 10^{16.9}$$ Equation 4-9

$$Am(OH)_3(cr) + 3H^+ \rightleftharpoons 3H_2O + Am^{3+}, K_{sp} = 10^{15.6}$$ Equation 4-10

The amorphous phase is roughly an order of magnitude more soluble than the crystalline one and will release more Am^{3+} into the system.

4.3 Carbonate Dissolution and Precipitation

CO_2 can be generated through the metabolic activity of microorganisms in the WIPP during CPR degradation (see Section 6.2.1). As a result of this reaction, the WIPP environment could become more acidic and could, in turn, increase actinide mineral solubility. The MgO engineered barrier is one way to control for this reaction and to buffer pH.

4.3.1 Henry's Law

CO_2 gas generated in the repository will interact with brine. Henry's Law describes the relationship between the partial pressure of a gas and the amount it will dissolve in a solution at a given temperature, described using the Henry's Law constant (K_H).

$$K_H = \frac{Gas\ Partial\ Pressure}{Moles\ of\ Dissolved\ Gas}$$ Equation 4-11

Table 4-1 shows K_H values for several gases relevant to the WIPP, in order of decreasing solubility. Of these gases, the most soluble gas is H_2S, whereas the least soluble gas is H_2. Various processes in the repository should be able to control an excess buildup of some gases. As previously discussed, CO_2 is controlled through the use of an engineered barrier, MgO, whereas H_2S and O_2 can be removed by corrosion of the iron canisters. Neither methane (CH_4) nor H_2 can be removed easily from the repository gas phase.

Gas	K_H (mol/L)	Source
H_2S	$10^{-0.96}$	Sander (2015)
CO_2	$10^{-1.5}$	Sander (2015)
CH_4	$10^{-2.8}$	Sander (2015)
O_2	$10^{-2.9}$	Sander (2015)
H_2	$10^{-3.1}$	Sander (2015)

Table 4-1. Henry's Law constants

4.3.2 The Carbonic Acid System

CO_2 dissolves in water to produce carbonic acid (H_2CO_3) through the following reaction:

$$CO_2(g) + H_2O(l) \rightleftharpoons H_2CO_3,\ K_H = \frac{a_{H_2CO_3}}{fCO_2} = 10^{-1.5}$$ Equation 3-10

(Recall that fugacity describes the gas's partial pressure in the atmosphere and is analogous to the concept of activity for gases.)

Acidity from the CO_2 is generated when H_2CO_3 dissociates and donates proton and bicarbonate (HCO_3^-) into solution:

$$H_2CO_3 \rightleftharpoons H^+ + HCO_3^-,\ K_1 = \frac{a_{H^+} \times a_{HCO_3^-}}{a_{H_2CO_3}} = 10^{-6.3}$$ Equation 4-12

HCO_3^- can further dissociate, donating a proton and carbonate ion to solutions:

$$HCO_3^- \rightleftharpoons H^+ + CO_3^{2-}, K_2 = \frac{a_{H^+} \times a_{CO_3^{2-}}}{a_{HCO_3^-}} = 10^{-10.3} \quad \text{Equation 4-13}$$

The combined concentrations of H_2CO_3, HCO_3, and carbonate (CO_3^{2-}) constitute the total inorganic carbon (TIC) of the system. Figure 4-3 shows the concentrations of each carbonate species in relation to a system's pH at atmospheric CO_2 fugacity of $10^{-3.5}$ atm and dilute solutions. Higher CO_2 fugacities will result in more H_2CO_3 generated and, subsequently, more acidity. This figure is in a log scale and shows that H_2CO_3, HCO_3^-, or CO_3^{2-} predominate as the main species contributing to TIC at different pH ranges.

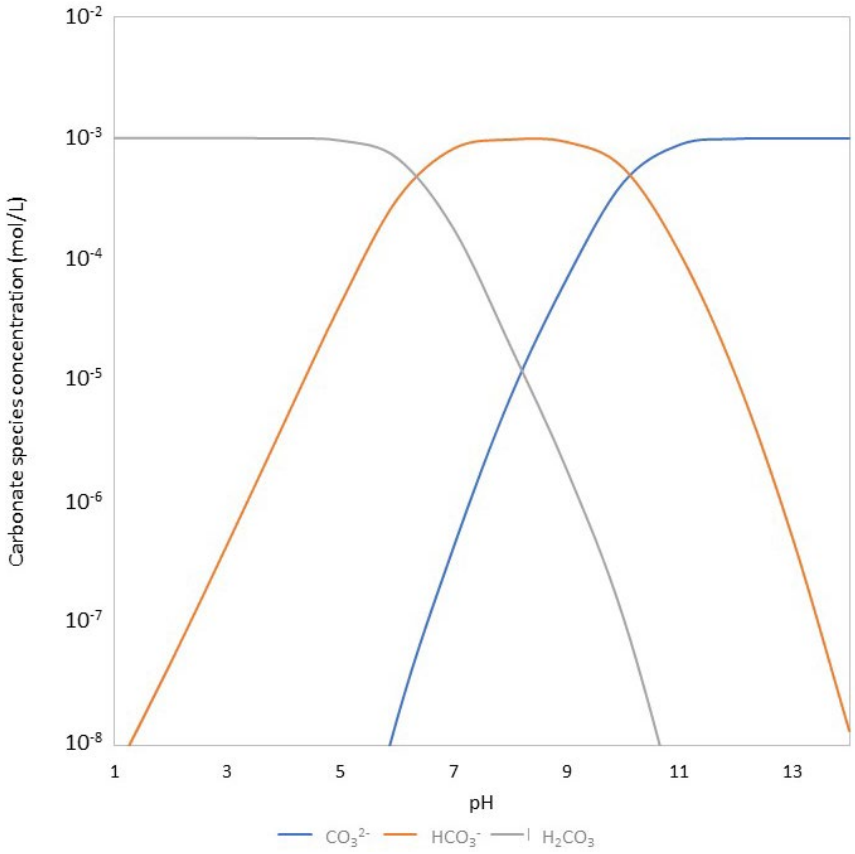

Figure 4-3. The carbonate system at 10^{-3} mol/L TIC and 10^{-3} mol/L NaCl at 1 atm, 25°C

At WIPP pH (between pH 8 and pH 10), we will expect to see CO_3^{2-} and HCO_3^- predominate the system. This is also the case at the ionic strengths characteristic for WIPP brines. These carbonate species readily form aqueous complexes with actinides, resulting in enhanced mobilization and making them important to include in calculating the actinide source term. These complexation reactions will be discussed in Section 4.3.

4.3.3 Mineral Interactions with CO_2 at the WIPP

4.3.3.1 Carbonates

Minerals can react with CO_2 and buffer the acidity it would normally generate. Through these reactions, H^+ is consumed as minerals are dissolved. Carbonate minerals, such as calcite and aragonite ($CaCO_3$), as well as dolomite ($CaMg(CO_3)_2$), are classic examples of this interaction. Calcite and aragonite can interact with CO_2 by combining the reactions below to describe the dissolution of this mineral:

$CaCO_3\ (s) \rightleftharpoons Ca^{2+} + CO_3^{2-}$ Equation 4-3

$H^+ + CO_3^{2-} \rightleftharpoons HCO_3^-$ Equation 4-13

$H_2CO_3 \rightleftharpoons H^+ + HCO_3^-$ Equation 4-12

$CO_2(g) + H_2O(l) \rightleftharpoons H_2CO_3$ Equation 3-10

$$CO_2(g) + H_2O(l) + CaCO_3(s) \rightleftharpoons Ca^{2+} + 2HCO_3^- \quad \text{Equation 4-14}$$

As salinity increases, the activities of Ca^{2+} and CO_3^{2-} will change because of the effects of ion-ion interactions. Because the ions at increased ionic strength have lower effective concentrations, more calcite is needed to dissolve to reach the constant value of K_{sp} of $10^{-8.34}$. As a result of this "salting in" effect, saline solutions increase dissolution of many carbonate minerals, shown in Figure 4-4:

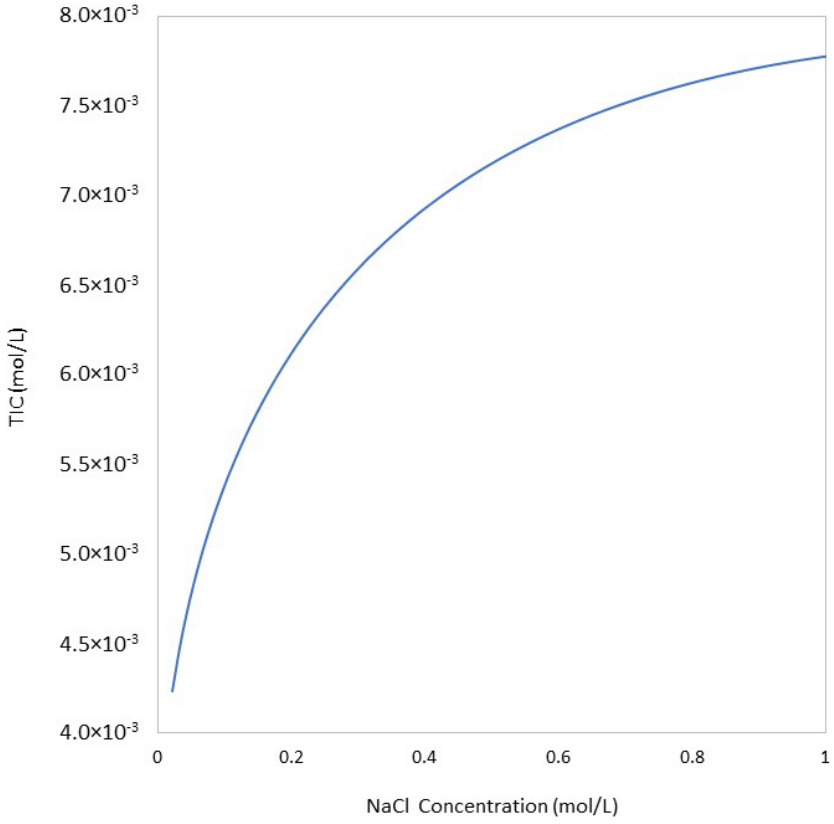

Figure 4-4. Ionic strength effects on calcite dissolution

The figure examines TIC and shows that with an increase in NaCl concentration (and ionic strength), more carbonate is dissolved. Carbonate minerals all follow a similar trend. Thus, a release into the Culebra could result in aggressive dissolution of the dolomite due to the "salting in" effect.

Other Acid-Base Systems

Many other systems follow similar speciation patterns as the carbonate system, such as phosphate, sulfate, sulfide, metal oxides, and borate. In these systems, the form that the ion of that species will take on will vary based on pH, with the most protonated being present at the lowest pH.

Borate ($B(OH)_3$) is an important system to the WIPP because it is present in brine (see Table 2-1). It also complexes with actinides, resulting in potentially enhanced mobilization. $B(OH)_3$ interacts with protons following the reaction (e.g., Snoyink and Jenkins 1980):

$$B(OH)_3 + H_2O \rightleftharpoons B(OH)_4^- + H^+, \qquad K = \frac{a_{B(OH)_4^-} \times a_{H^+}}{a_{B(OH)_3}} = 10^{-9.3}$$

Unlike the previous reactions, where we see the carbonate species donate H^+, $B(OH)_3$ accepts a hydroxide from water $(OH)^-$, to make $B(OH)_4^-$.

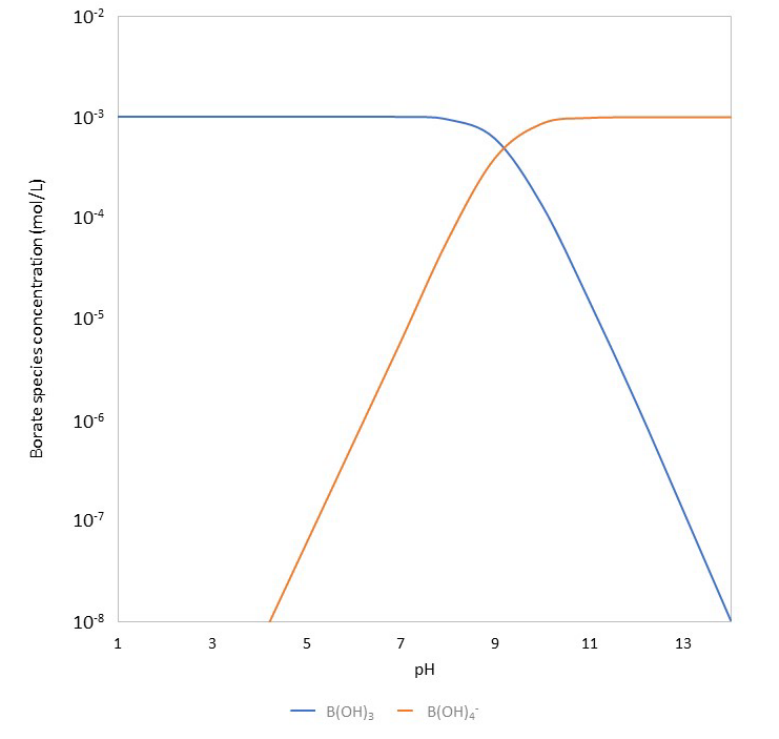

Borate is a particularly tricky element to study as a result of its ability to form polyborates at high concentrations. Polyborates include such species as $B_3O_3(OH)_4^-$ and $B_5O_6(OH)_4^-$. Multiple minerals also may contribute to $B(OH)_3$ dissolution and precipitation in brine, such as $Na_2B_4O_7{\bullet}10H_2O$, and do not necessarily separate specifically into simply two Na^+ and one $B_4O_7^{2-}$ (also referred to as incongruent dissolution).

Box 4-2. Other acid-base systems

4.3.3.2 Magnesium Oxide

Because the acidity created by CO_2 in the repository has such important implications toward actinide solubility, the WIPP uses an engineered barrier to absorb any CO_2 gas generated. This engineered barrier is composed of an MgO backfill, which is added as supersacks, or large bags of stacked MgO on waste containers (Figure 4-5). MgO is added in an excess relative to the amount of carbon that is estimated to be present, calculated to provide more than enough reactant to absorb any potential CO_2.

Figure 4-5. MgO supersacks placed on waste canisters. Red arrows showing the MgO supersacks placed on waste canisters. Adapted from Figure 1 of Appendix MgO (DOE 2014a)

The MgO reacts with CO_2 through multiple steps during the repository's lifetime. Within several hours to several days on brine contact, the MgO will rapidly react and form brucite, $Mg(OH)_2$.

$$MgO(s) + H_2O(l) \rightleftharpoons Mg(OH)_2(s) \quad \text{Equation 4-15}$$

Subsequently, within several hours to several days, the $Mg(OH)_2$ then will convert into hydromagnesite, $Mg_5(CO_3)_4(OH)_2 \cdot 4H_2O$:

$$5Mg(OH)_2(s) + 4CO_2(g) \rightleftharpoons Mg_5(CO_3)_4(OH)_2 \cdot 4H_2O(\text{s}) \quad \text{Equation 4-16}$$

Over longer time scales (i.e., hundreds to thousands of years), the $Mg_5(CO_3)_4(OH)_2 \cdot 4H_2O$ will turn into magnesite $MgCO_3$:

$$Mg_5(CO_3)_4(OH)_2 \cdot 4H_2O(\text{s}) + CO_2(g) \rightleftharpoons 5Mg(CO)_3(s) + 5H_2O(l) \quad \text{Equation 4-17}$$

Note that when MgO is converted into $Mg(OH)_2$, water is consumed. During the conversion of $Mg(OH)_2$ to $MgCO_3 \cdot 3H_2O$, H_2O is consumed in addition to CO_2. When $Mg_5(CO_3)_4(OH)_2 \cdot 4H_2O$ is produced, CO_2 is produced. When $Mg_5(CO_3)_4(OH)_2 \cdot 4H_2O$ converts to $MgCO_3$, CO_2 is consumed and water is produced. In the case of the engineered barrier, the rates of reaction matter because it will influence the amount of CO_2 consumed, as well as the repository water balance over 10,000 years. $Mg_5(CO_3)_4(OH)_2 \cdot 4H_2O$ itself is a metastable mineral (i.e., it is thermodynamically unstable, but because of its persistence over long time scales, it may essentially be modeled as a stable mineral). Because of the mineral's potentially long conversion rate into magnesite, the WIPP PA samples multiple reaction rates.

Besides removing CO_2 from the repository, MgO has the added benefit of buffering the pH of the system by consuming protons. This will happen when $Mg(OH)_2$ consumes H^+:

$$Mg(OH)_2(s) + H^+ \rightleftharpoons Mg^{2+} + 2H_2O(l) \quad \text{Equation 4-18}$$

Other MgO Hydration and Carbonation Products

Prior to the carbonation of MgO minerals to hydromagnesite, MgO will hydrate upon reaction with brine and form minerals such as brucite (Equation 4-15), phase 5 [$Mg_3(OH)_5Cl{\bullet}4H_2O$], and phase 3 ($Mg_2Cl(OH)_3{\cdot}4H_2O$). Also known as "Sorel cements," both phase 5 and phase 3 are important because their precipitation removes water from the environment, as shown in the reactions below. Of the Sorel cements, DOE has found that phase 5 is the likeliest to be at WIPP, though experimental evidence suggests its precipitation will be limited.

Phase 5: $3MgO(s) + H^+ + Cl^- + 6H_2O \leftrightharpoons Mg_3(OH)_5Cl{\bullet}4H_2O(s)$

Phase 3: $2MgO(s) + H^+ + Cl^- + 5H_2O \leftrightharpoons Mg_2Cl(OH)_3{\bullet}4H_2O(s)$

Reaction of MgO minerals with CO_2 results in carbonation. Although the carbonation of brucite to magnesite is predicted, DOE has investigated the potential presence of other intermediate metastable phases, including nesquehonite and two forms of hydromagnesite. The hydromagnesite in Equation 4-16 is also known as hydromagnesite5424. Another form of hydromagnesite examined at WIPP is hydromagnesite4323 ($Mg_4(CO_3)_3(OH)_2{\bullet}3H_2O$). The brucite carbonation reactions into nesquehonite and hydromagnesite4323 are shown below:

Nesquehonite: $Mg(OH)_2(s) + CO_2(g) + 2H_2O \leftrightharpoons MgCO_3{\bullet}3H_2O(s)$

Hydromagnesite4323: $4Mg(OH)_2(s) + 3CO_2(g) \leftrightharpoons Mg_4(CO_3)_3(OH)_2{\bullet}3H_2O(s)$

The formation of carbonated MgO phases is extremely important in the WIPP PA as some reactions are more effective at buffering CO_2 than others. For example, hydromagnesite5424 maintains lower CO_2 partial pressures and actinide solubilities than nesquehonite. Of the three metastable hydrated MgO phases discussed, the most likely phase to exist at the WIPP is hydromagnesite5424, which also happens to be the most effective at buffering CO_2 and the resulting effects on actinide solubility.

Box 4-3. Other MgO hydration and carbonation products

5 Complexation

Actinides in solutions do not exist just as naked ions. Ions in solution may attach to each other as aqueous complexes. This influences the amount of an actinide solid that may dissolve, affects the amount of free metal ions available for sorption or precipitation reactions, and alters the total actinide concentrations in solution. For example, actinides may interact with carbonate ions in solution, with organic ligands, or even with water, creating complexes that increase total actinide concentrations in solution. Actinides may interact with themselves, forming long chains of macromolecules known as colloids (see Section 5.4), which also will contribute to an increase in mobilized actinides. Complexation reactions are important for tracking the fate and transport of actinides in brine and contribute to WIPP geochemical models that determine potential releases. These reactions provide insight into actinide solubility behavior and the conditions at which solubility can be kept at a minimum.

5.1 Stability Constants

To calculate how stable a complex will be, we utilize stability constants, β or log β (note that this β value is different from the Pitzer parameter with the same nomenclature). Stability constants are calculated the same way as other equilibrium constants (i.e., K values). For example, if ions A^+ and B^- form the complex AB, we can write the reaction as the association of the two ions, represented below:

$$A^+ + B^- \rightleftharpoons AB(aq), \beta_1 = \frac{a_{AB}}{a_{A^+} \times a_{B^-}} \quad \text{Equation 5-1}$$

Multiple B^- anions could complex with the A^+ cation, and these would be represented with successive β values (e.g., β_2, β_3):

$$A^+ + 2B^- \rightleftharpoons AB_2^-(aq), \beta_2 = \frac{a_{AB_2^-}}{a_{A^+} \times a_{B^-}^2} \quad \text{Equation 5-2}$$

$$A^+ + 3B^- \rightleftharpoons AB_3^{2-}(aq), \beta_3 = \frac{a_{AB_3^{2-}}}{a_{A^+} \times a_{B^-}^3} \quad \text{Equation 5-3}$$

The opposite of a stability constant is an instability constant, also known as a dissociation constant (represented as K or log K). This is the form we have seen previously when we examined mineral dissolution reactions or the dissociations of acids like H_2CO_3. In these reactions, we see the inverse of stability constants (i.e., the complex or solid is the reactant, and the ions are the products).

Am^{3+} is one WIPP-relevant actinide that participates in a number of complexation reactions. For example, Am^{3+} may associate with Cl^- in WIPP brine to form the americium-chloride complexes $AmCl^{2+}$ and $AmCl_2^+$ in the following reactions (DOE 2014c):

$$Am^{3+} + Cl^- \rightleftharpoons AmCl^{2+}, \beta_1 = \frac{a_{AmCl^{2+}}}{a_{Am^{3+}} \times a_{Cl^-}} = 10^{0.24} \quad \text{Equation 5-4}$$

$$Am^{3+} + 2Cl^- \rightleftharpoons AmCl_2^+, \beta_2 = \frac{a_{AmCl_2^+}}{a_{Am^{3+}} \times a_{Cl^-}^2} = 10^{-0.74} \quad \text{Equation 5-5}$$

With stability constants, the higher the number, the more stable the complex. In this case, $AmCl^{2+}$ is more stable than $AmCl_2^+$. Note, Equation 5-2 also can be written as

$$AmCl^{2+} + Cl^- \rightleftharpoons AmCl_2^+$$

However, Equation 5-2 provides an overall formation reaction for $AmCl^{2+}$ by using only the reactants Am^{3+} and Cl^-. This is especially useful for calculating complex formation during geochemical modeling because it simplifies the reaction and uses previously defined species.

Complexation reactions will happen between different ions in a solution. Cl^- in the above reactions, for example, will complex with other ions—such as Na^+, Ca^{2+}, Mg^{2+}, etc.—as well as any metals and actinides. $B(OH)_3$, SO_4^{2-}, H_2O, CO_3^{2-}, and many other components also will form complexes. Metals and actinides, such as Th, may even complex with themselves. A few example complexation reactions are provided below.

5.2 Metal and Actinide Hydrolysis

Hydrolysis occurs when free metal ions form a complex with water. Oxidized iron metal from waste containers, for example, can interact with H_2O, removing OH^- ions from the H_2O, adding protons into the solution, and forming an aqueous complex as a result (e.g., Appello and Postma 2005):

$$Fe^{3+} + H_2O \rightleftharpoons Fe(OH)^{2+} + H^+, \beta_1 = \frac{a_{Fe(OH)^{2+}} \times a_{H^+}}{a_{Fe^{+3}}} = 10^{-2.19} \quad \text{Equation 5-6}$$

$$Fe^{3+} + 2H_2O \rightleftharpoons Fe(OH)_2^+ + 2H^+, \beta_2 = \frac{a_{Fe(OH)_2^+} \times a_{H^+}^2}{a_{Fe^{+3}}} = 10^{-5.67} \quad \text{Equation 5-7}$$

$$Fe^{3+} + 3H_2O \rightleftharpoons Fe(OH)_3^0 + 3H^+, \beta_3 = \frac{a_{Fe(OH)_3^0} \times a_{H^+}^3}{a_{Fe^{+3}}} = 10^{-12.56} \quad \text{Equation 5-8}$$

$$Fe^{3+} + 4H_2O \rightleftharpoons Fe(OH)_4^- + 4H^+, \beta_4 = \frac{a_{Fe(OH)_4^-} \times a_{H^+}^4}{a_{Fe^{+3}}} = 10^{-21.6} \quad \text{Equation 5-9}$$

Figure 5-1 shows the relationship between these complexes and pH, assuming no precipitation. It shows that Fe^{3+} concentrations are at their maximum between pH 1–3. At higher pH values, Fe^{3+} ion concentrations quickly decrease, making very little contribution to the total iron in solution. Because of its extremely low concentration, Fe^{3+} essentially can be ignored at high pH values.

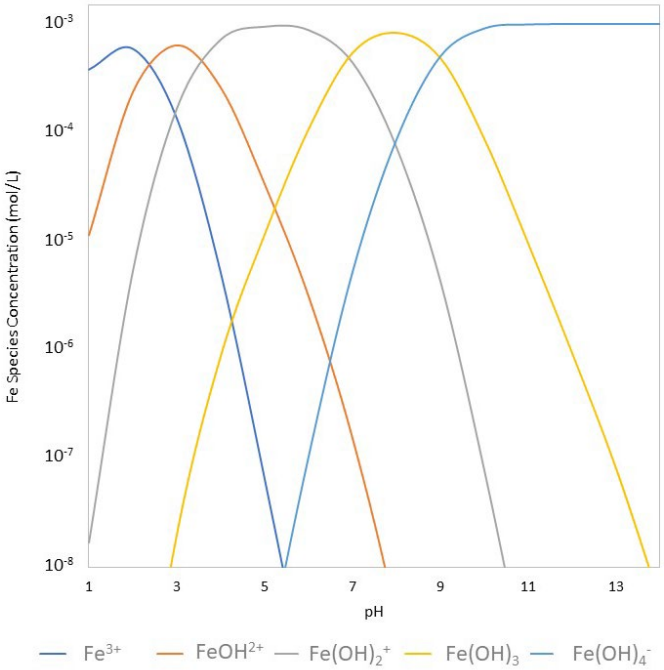

Figure 5-1. Speciation of 0.001 M Fe^{3+} in 0.001 M NaCl, assuming no precipitation

Actinides readily hydrolyze as well. Using the example from Figure 3-1, we see that that the total Np(V) in solution is composed of NpO_2^+, as well as $NpO_2OH(aq)$ and $NpO_2(OH)_2^-$. This is because NpO_2^+ reacts with water to form hydrolysis species (Guillaumont et al. 2003).

$$NpO_2^+ + H_2O \rightleftharpoons NpO_2OH(aq) + H^+, \beta_1 = \frac{[NpO_2OH][H^+]}{[NpO_2^+]} = 10^{-11.3} \text{ Equation 5-10}$$

$$NpO_2^+ + 2H_2O \rightleftharpoons NpO_2(OH)_2^- + 2H^+, \beta_2 = \frac{[NpO_2OH^{-2}][H^+]^2}{[NpO_2^+]} = 10^{-23.6} \text{ Equation 5-11}$$

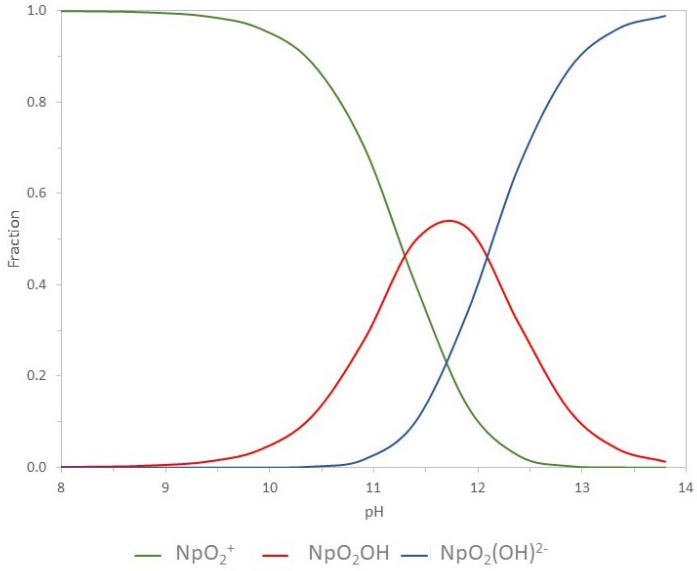

Figure 5-2. Fractional diagram of Np(V)

Metal speciation can be represented as a fractional diagram (Figure 5-2), which illustrates the fractional contribution of each species of Np(V) to total Np(V) over a pH range.

Thorium is another actinide that readily hydrolyzes, making it difficult and complicated to study. In this case, the higher β values compared to Np(V) show that Th hydrolysis complexes are far more stable and hydrolyze at much lower pH. This makes laboratory quantification particularly tricky (Rand et al. 2009).

$$Th^{4+} + H_2O \rightleftharpoons Th(OH)^{3+} + H^+ \qquad \beta_1 = \frac{a_{Th(OH)^{3+}} \times a_{H^+}}{a_{Th^{+4}}} = 10^{-2.5} \text{ Equation 5-12}$$

$$Th^{4+} + 2\,H_2O \rightleftharpoons Th(OH)_2^{2+} + 2\,H^+ \qquad \beta_2 = \frac{a_{Th(OH)_2^{2+}} \times a_{H^+}^2}{a_{Th^{+4}}} = 10^{-6.2} \text{ Equation 5-13}$$

$$Th^{4+} + 3\,H_2O \rightleftharpoons Th(OH)_3^{+} + 3\,H^+ \qquad \beta_3 = \frac{a_{Th(OH)_3^{+}} \times a_{H^+}^3}{a_{Th^{+4}}} = 10^{-11.0} \text{ Equation 5-14}$$

$$Th^{4+} + 4\,H_2O \rightleftharpoons Th(OH)_4^{0} + 4\,H^+ \qquad \beta_4 = \frac{a_{Th(OH)_4^{0}} \times a_{H^+}^4}{a_{Th^{+4}}} = 10^{-17.4} \text{ Equation 5-15}$$

This is highlighted in Figure 5-3, showing the fractional contribution of Th(IV) hydrolysis species. Note that unlike Np(V), the Th(IV) species are present at a lower pH range. For Np(V), hydrolysis species

appear within the pH ranges of 9–14 (Figure 5-2), whereas Th(IV) species appear between pH 1 and 8 (Figure 5-3). Additionally, the free Th^{4+} ion only predominates at a pH between 1 and 3.

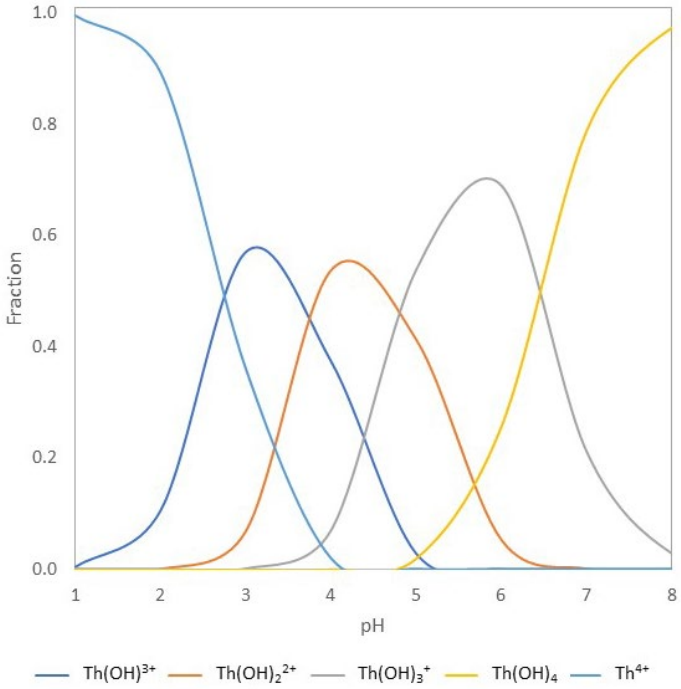

Figure 5-3. Fractional diagram of Th(IV) at 0.001 M NaCl and 0.001 M total Th(IV)

5.3 Carbonate Complexation

Because actinide-carbonate complexes are highly stable, the total inorganic carbon (TIC) can have important implications for the extent of actinide dissolution in the WIPP. Uranium is an example of an actinide that can form strong complexes with carbonate. In its oxidized form, U(VI), uranium exists in aqueous solutions as UO_2^{2+}. This ion will complex with carbonate with the following reactions (Guillaumont et al. 2003):

$$UO_2^{2+} + CO_3^{2-} \rightleftharpoons UO_2CO_3(aq), \beta_1 = \frac{a_{UO_2CO_3}}{a_{UO_2^{2+}} \times a_{CO_3^{2-}}} = 10^{9.94} \quad \text{Equation 5-16}$$

$$UO_2^{2+} + 2CO_3^{2-} \rightleftharpoons UO_2(CO_3)_2^{2-}, \beta_2 = \frac{a_{UO_2(CO_3)_2^{2-}}}{a_{UO_2^{2+}} \times a_{CO_3^{2-}}^2} = 10^{16.61} \quad \text{Equation 5-17}$$

$$UO_2^{2+} + 3CO_3^{2-} \rightleftharpoons UO_2(CO_3)_3^{4-}, \beta_3 = \frac{a_{UO_2(CO_3)_3^{4-}}}{a_{UO_2^{2+}} \times a_{CO_3^{2-}}^3} = 10^{21.84} \quad \text{Equation 5-18}$$

$$3UO_2^{2+} + 6CO_3^{2-} \rightleftharpoons (UO_2)_3(CO_3)_6^{6-}, \beta_4 = \frac{a_{UO_2(CO_3)_6^{6-}}}{a_{UO_2^{2+}} \times a_{CO_3^{2-}}^6} = 10^{54.0} \quad \text{Equation 5-19}$$

Note the increasingly large positive exponents in the β values, indicating high stability. These numbers also are larger in comparison to hydrolysis constants of UO_2^{2+}:

$$UO_2^{2+} + H_2O \rightleftharpoons UO_2(OH)^+ + H^+, \beta_1 = \frac{a_{UO_2(OH)^+} \times a_{H^+}}{a_{UO_2^{2+}}} = 10^{-5.2} \quad \text{Equation 5-20}$$

$$UO_2^{2+} + 2H_2O \rightleftharpoons UO_2(OH)_2 + 2H^+, \beta_2 = \frac{a_{UO_2(OH)_2} \times a_{H^+}^2}{a_{UO_2^{2+}}} = 10^{-12.1} \quad \text{Equation 5-21}$$

$$UO_2^{2+} + 3H_2O \rightleftharpoons UO_2(OH)_3^- + 3H^+, \beta_3 = \frac{a_{UO_2(OH)_3^-} \times a_{H^+}^3}{a_{UO_2^{2+}}} = 10^{-20.25} \quad \text{Equation 5-22}$$

$$UO_2^{2+} + 4H_2O \rightleftharpoons UO_2(OH)_4^{2-} + 4H^+, \beta_3 = \frac{a_{UO_2(OH)_4^{4-}} \times a_{H^+}^4}{a_{UO_2^{2+}}} = 10^{-32.4} \quad \text{Equation 5-23}$$

For U and many other metals, the addition of carbonates changes the distribution of total metal species in solution. As shown in Figure 5-4, the addition of 0.001 M TIC to a dilute NaCl solution containing 0.001 M total U results in the dominance of uranium-carbonate complexes between the pH values of approximately 5–10. The UO_2^{2+} ion exists only in acidic conditions (declining rapidly at pH above 4). Hydrolysis becomes important at extremely high pH.

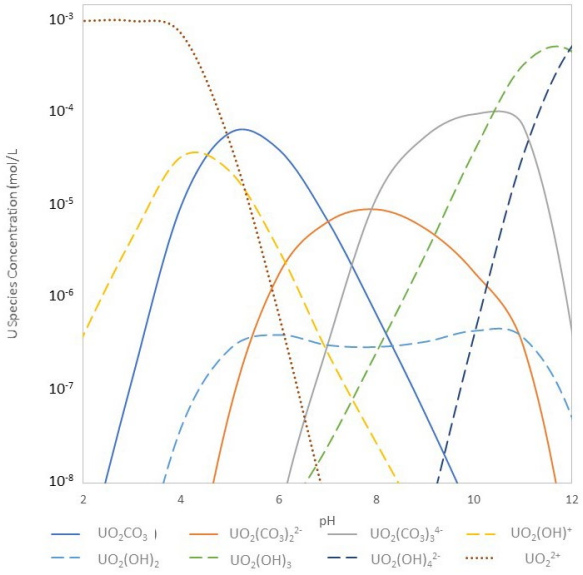

Figure 5-4. The distribution of uranyl ion (UO_2^{2+}) and complexes in a 0.001 M NaCl solution containing 0.001 TIC and 0.001 M total uranium

5.4 Complexation of Macromolecules

5.4.1 Organic Ligands

Organic compounds form strong complexes with metals and actinides. These large molecules often have multiple binding sites, allowing them to attach to a metal at multiple locations. As a result, organic ligands, or chelates, tend to form very stable complexes (see Box 5-1 for more details).

Chelates can increase the solubility of a metal. Some important organic compounds associated with the WIPP include ethylenediaminetetraacetic acid (EDTA, $C_{10}H_{16}N_2O_8^{4-}$), oxalate ($C_2O_4^{2-}$), citrate ($C_6H_8O_7$), and acetate ($C_2H_3O_2^-$). Many of these compounds are present in cleanup activities and thus are contaminants in the WIPP waste that are important to consider in PA calculations. $C_2O_4^{2-}$, $C_6H_8O_7$, and $C_2H_3O_2^-$ are organic molecules that microorganisms can degrade quickly, but it is likely EDTA will persist for longer. Table 5-1 lists stability constants for some WIPP-relevant actinides associated with EDTA. Because Pu is expected to contribute the most to repository releases, and because of its high complexation with EDTA, understanding Pu-EDTA interactions is especially important to consider in the WIPP PA. Besides increasing the amounts dissolved concentrations of Pu in solution, EDTA may also further aid in oxidation-reduction reactions that further increase dissolved Pu. See Section 6.2.3 for more

details. Note the large positive numbers on all the constants, showing that these complexes are extremely stable.

Actinide	Reaction	Stability Constant	Source
Am(III)	$Am^{3+} + EDTA^{4-} \rightleftharpoons AmEDTA^{-}$	19.67	Hummel et al. (2005)
Pu(III)	$Pu^{3+} + EDTA^{4-} \rightleftharpoons PuEDTA^{-}$	20.18	Hummel et al. (2005)
Th(IV)	$Th^{4+} + EDTA^{4-} \rightleftharpoons ThEDTA$	26.95	Grive et al. (2014)
Np(V)	$NpO_2^{+} + EDTA^{4-} \rightleftharpoons NpO_2EDTA^{3-}$	9.23	Hummel et al. (2005)
U(VI)	$UO_2^{2+} + EDTA^{4-} \rightleftharpoons UO_2EDTA^{2-}$	13.7	Hummel et al. (2005)

Table 5-1. Organic ligand stability constants with WIPP-relevant actinides

5.4.2 Humic Colloids

Humic substances are large, complex, and extremely diverse organic macromolecules. These substances are the result of the biodegradation of even larger organic molecules and have ill-defined molecular structures and physical and chemical characteristics. These molecules also can be much larger than organic ligands, such as EDTA, with molecular weights from hundreds to tens of thousands of kilodaltons.[2]

In the WIPP, humic substances are defined as hydrophilic, soft-sphere particles that are stabilized by solvation forces in water (DOE 2014c). Owing to their large sizes, humic substances have many different functional groups associated with them, giving them the potential to chelate a considerable number of metals. Consequently, humic substances easily can bind metals and bring them into solution, making them a contributor to the actinide source term. An example of a complexation reaction between a humic acid (Hs^{-}) and an actinide (Am^{3+}) is presented below (DOE 2019b):

$$Am^{3+}Hs^{-} \rightleftharpoons AmHs^{2+}, \beta = \frac{AmHs^{2+}}{Am^{3+} \times Hs^{-}} = 10^{6.09} \quad \text{Equation 5-24}$$

Because humic substances are so diverse, no one humic substance can completely represent the universe of such substances. Instead, experiments to understand their solubility and complexation properties rely on model humic compounds. In the WIPP, these models are humic and fulvic acids from the Suwannee River, Georgia; from Gorleben, Germany; from Lake Bradford, Florida; and from various vendors, such as Aldrich Chemical Co. (Papenguth 1996). Experiments to understand their contribution to the actinide source term provide information on the proportion of actinides in solutions that will be bound to humics. These data result in a proportionality constant, which is used to calculate the humic colloid contribution to the source term.

5.4.3 Intrinsic Colloids

Actinides also can form complexes with themselves, creating long chains of macromolecules, referred to as intrinsic colloids or eigencolloids (Papenguth and Behl 1996). During hydrolysis, an actinide—such as Pu—will react with water to form a complex:

$$Pu^{4+} + 2H_2O \rightleftharpoons Pu(OH)_2^{2+} + 2H^{+} \quad \text{Equation 5-25}$$

The $Pu(OH)_2^{2+}$ complex can continue to complex with itself to form a polymer, such as

$$Pu(OH)(OH)Pu(OH)(OH)Pu(OH)(OH)Pu(OH)(OH)\ldots$$

[2] A Dalton is defined as 1/12 of the mass of an unbound neutral atom of carbon-12 in its nuclear and electronic ground state and at rest. One kilodalton is the equivalent of approximately 1.6605×10^{-21} grams.

Over time, the polymer matures, resulting in the removal of H_2O from the macromolecule, also referred to as olation:

$$Pu(OH)(OH)Pu(OH)(OH)Pu(OH)(OH)Pu(OH)(OH) \rightleftharpoons Pu(O)Pu(O)Pu(O)Pu(O) + 4\ H_2$$

Immature intrinsic colloids are hydrophilic and can remain in solution; however, as these molecules mature, they may become hydrophobic and could potentially precipitate into a mineral. Because of the

Coordination Chemistry

Complex formation can be the result of ion interactions that are electrostatic, covalent, or mixed. The metal cation involved in the coordination compound is referred to as the central atom, whereas the anions and other molecules binding to the central atom are the ligands.

Ligands can attach to the atoms at multiple sites. Monodentate ligands, such as Cl^- and OH^-, attach to the central atom at one location. Other ligands, such as SO_4^{2-}, could be bidentate, attaching to a metal ion (M) at two locations:

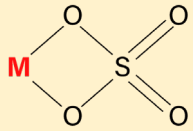

EDTA is an example of a multidentate ligand because it has six sites that allow it to bind to a metal atom:

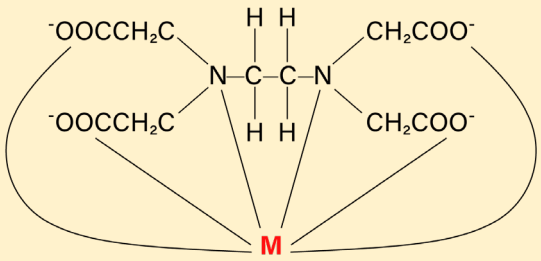

Larger organic molecules, such as humic acids, although ill-defined, have different functional groups present in their molecular structures that give them the ability to bind to metals. These include carboxyl, phenolic, alcohol, methoxyl, carbonyl, ether, and ester groups shown below.

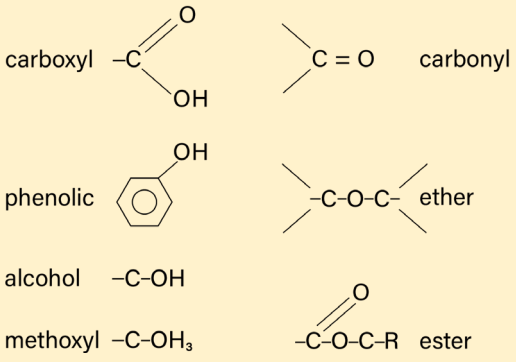

Box 5-1. Coordination chemistry

tendency for actinides to form macromolecules, the WIPP colloidal actinide source term also considers intrinsic colloids in the total amount of actinides that can be present during a release. Precipitated actinide molecules also are a component of the mineral fragment colloids model. See Section 7.3.1 for more details on these types of colloids.

6 Oxidation-Reduction Reactions

Oxidation-reduction or redox reactions can be described as the transfer of electrons from a species that donates an electron (reductant) to a species that accepts an electron (oxidant). Once a species accepts an electron, it is reduced and its valence state decreases. For example, Pu^{4+} and Fe^{3+} are oxidized forms of plutonium and iron relative to the reduced forms Pu^{3+} and Fe^{2+}. These valence states also can be expressed as roman numerals (e.g., Pu(IV), Fe(III), Pu(III), Fe(II)). Different redox conditions in the repository will favor these various valence states.

Among actinides, redox reactions can be extremely complicated. For example, plutonium can be present in multiple different oxidation states in the environment, Pu^{6+}, Pu^{5+}, Pu^{4+}, and Pu^{3+}. Each state has its own set of complexation reactions and solubility. At the WIPP, redox is vitally important to consider because the redox conditions in the repository will control which actinide oxidation states will dominate, affecting the overall solubility and source term. Redox conditions in the repository are controlled by many different processes, ranging from microbial activity to iron corrosion to actinide radiolysis. In this section, we describe the fundamentals of redox reactions and how they relate to the WIPP.

6.1 Oxidation Reduction Reactions

In the following reduction reaction, an iron oxide, ferrihydrite ($Fe(OH)_3(s)$), accepts an electron (e^-). As a result, it is reduced to aqueous ferrous iron, Fe^{2+}.

$$Fe(OH)_3(s) + 3H^+ + e^- \rightleftharpoons Fe^{2+} + 3H_2O \quad \text{Equation 6-1}$$

An example of an oxidation reaction is the oxidation of H_2. In this case, $H_2(g)$ donates two electrons. Doing so oxidizes it into two protons (H^+) and two electrons.

$$H_2(g) \rightleftharpoons 2H^+ + 2e^- \quad \text{Equation 6-2}$$

In reality, free electrons do not exist in aqueous solutions. To correctly represent redox reactions, we can combine the two half reactions presented. The result is the reduction of the iron solid into ferrous iron by $H_2(g)$.

$$2Fe(OH)_3(s) + H_2(g) + 4H^+ \rightleftharpoons 2Fe^{2+} + 6H_2O \quad \text{Equation 6-3}$$

Redox Half Reactions

Reduction Half Reactions:

$O_2 + 4H^+ + 4e^- \rightleftharpoons 2H_2O$

$SO_4^{2-} + 9H^+ + 8e^- \rightleftharpoons HS^- + 4H_2O$

$CO_2 + 8H^+ + 8e^- \rightleftharpoons CH_4 + 2H_2O$

$PuO_2 + 4H^+ + e^- \rightleftharpoons Pu^{3+} + 2H_2O$

Oxidation Half Reactions:

$C_6H_{10}O_5 + 7H_2O \rightleftharpoons 6CO_2 + 24H^+ + 24e^-$

$Fe^0 \rightleftharpoons Fe^{2+} + 2e^-$

Box 6-1. Redox half reactions

A complete expression involves the combination of both oxidation and reduction half reactions. Box 6-1 lists a few other important half reactions to WIPP.

6.1.1 Redox Potentials

The redox potential of a system is a relative measure of its oxidation-reduction state, referred to as E_H. Units for this measure are in volts because the number is derived from the flow of electrons through a hypothetical platinum electrode. High potentials tend to favor oxidizing valence states and can be referred to as oxidizing environments. Lower potentials tend to favor reduced valence states and can be referred to as reducing environments.

Converting Between pe and E_H

The Nernst equation can be expressed as

$$pe = \frac{F}{2.303\ RT} E_H$$

where

F = Faraday's constant
R = the gas constant
T = temperature

and 2.303 is the conversion from natural to base 10 logarithms.

Box 6-2. Converting between pe and E_H

Alternatively, redox potentials also can be measured through the negative logarithm of electron activity, pe, which describes the activity of an electron, analogous to the concept of pH. Both pe and E_H are related through the Nernst equation (Box 6-2) and can be converted interchangeably.

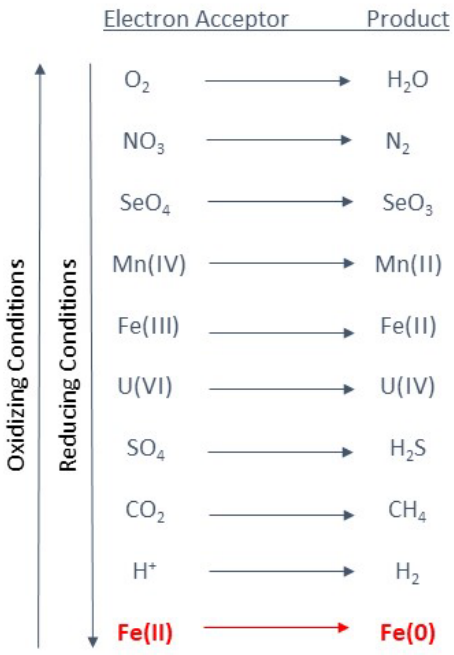

Figure 6-1. The redox ladder

Some aqueous species have higher affinities for accepting electrons, whereas other species will tend to donate electrons. Redox potential helps us order which species have the greatest affinity for accepting or donating electrons. Species relevant to the WIPP can be ordered using the *redox ladder* shown in Figure 6-1.

As seen in Equations 6-1 to 6-3, redox reactions also have a relationship with H^+. This means many redox reactions also are pH dependent. This relationship can be represented in a stability diagram, as in Figure 6-2 (Schramke et al. 2020).

The stability diagram describes the relationship of a set quantity of Pu and its prevailing speciation or oxidation state based on the redox chemistry of the environment. The diagram illustrates redox conditions at 0.1 *m* NaCl and at 1 atm pressure. The oxidizing conditions are greatest at 1 atm of pure O_2 gas, whereas the reducing conditions are greatest at 1 atm of pure H_2 gas. Note that WIPP pressures are expected to exceed 150 atm and, consequently, the pe or E_H ranges likely will increase as the pressure expands the lower boundary of the pe values (dashed line in Figure 6-2; see Schramke et al. 2020 for more information).

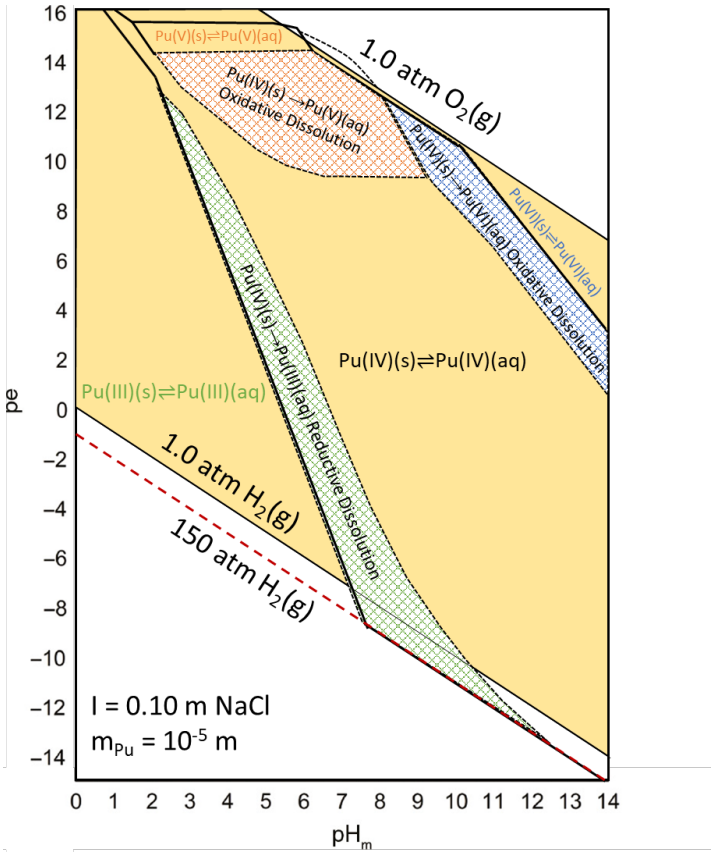

Figure 6-2. Stability diagram of Pu(III) and Pu(IV) calculated at 0.1 m *NaCl and at 1 atm (Adapted from Schramke et al. 2020)*

Stability diagrams help us visualize and predict which redox-sensitive mineral phases are most stable at a given condition. This is important because different redox conditions will favor phases of Pu that will be more soluble than others and can contribute to a higher release.

6.2 WIPP-Relevant Redox Reactions

Redox reactions are vital to WIPP geochemistry and have implications toward multiple repository processes, including CPR degradation, gas generation, and pH and the speciation and solubility of actinides.

6.2.1 Microbial Respiration

Respiration is a redox reaction catalyzed by organisms. Energy is transferred when a substrate, usually an organic compound, is oxidized and an electron acceptor is reduced. Cellulose (such as the monomer $C_6H_{10}O_5$) is an important example of an electron donor at the WIPP that can provide energy to microorganisms. Its oxidation results in the

generation of CO_2, which has implications for both repository gas pressures and pH. Hydrogen gas also can donate electrons. Below are a few examples of important redox reactions at the WIPP. These reactions have been combined from the half reactions presented in Box 6-1. Of these reactions, aerobic respiration occurs the fastest and also will yield the highest amount of energy for organisms. The amount of energy provided from organic carbon oxidation then will decrease following the order of the redox ladder (Figure 6-1).

- Aerobic respiration

$$6O_2 + C_6H_{10}O_5 \rightleftharpoons 6CO_2 + 5H_2O \text{ Equation 6-4}$$

- Nitrate reduction

$$4.8NO_3^- + C_6H_{10}O_5 + 4.8\,H^+ \rightleftharpoons 6CO_2 + 7.4H_2O + 2.4N_2 \text{ Equation 6-5}$$

- Sulfate reduction

$$3SO_4^{2-} + C_6H_{10}O_5 + 6H^+ \rightleftharpoons 3H_2S + 6CO_2 + 5H_2O \text{ Equation 6-6}$$

$$SO_4^{2-} + 4H_2 + 2H^+ \rightleftharpoons H_2S + 4H_2O \text{ Equation 6-7}$$

- Methanogenesis

$$CO_2 + 4H_2 \rightleftharpoons CH_4 + 2H_2O \text{ Equation 6-8}$$

$$C_6H_{10}O_5 + H_2O \rightleftharpoons 3CH_4 + 3CO_2 \text{ Equation 6-9}$$

As with the reactions above, the WIPP PA considers the microbial oxidation of other carbon compounds in the CPR, although the amount of CO_2 released will depend on the complexity of the carbon compound being oxidized. After the repository is sealed, we can expect aerobic respiration to quickly consume all the available O_2 in the repository at the time of closure. This will cause a decrease in repository E_H. In the absence of any other potential electron acceptors, nitrate reduction, sulfate reduction, and methanogenesis will become the microbial respiration processes.

H_2 also can be oxidized to provide energy. During sulfate reduction, H_2 transfers its electron to SO_4^{2-}, creating H_2S gas as a byproduct. In methanogenesis, H_2 transfers its electron to CO_2, resulting in CH_4. H_2S gas is removed from solution through the corrosion of iron in the waste canisters (Equation 6-11), although some gas still may contribute to repository pressure increases. Methane is highly insoluble and will contribute only to an increase in repository pressure, which—if buildup were to occur in the WIPP—could aid in a direct brine release (DBR). Fortunately, because of the abundance of sulfate in the WIPP from the anhydrite interbeds, sulfate reducers have a nearly inexhaustible electron acceptor source. Thus, sulfate-reducing microorganisms will be able to outcompete methanogens and prevent the buildup of CH_4.

6.2.2 Iron Corrosion

Hydrogen gas is an important component in WIPP redox reactions. The H_2 responsible for reducing sulfate and carbon dioxide in Equations 6-7 and 6-8 may be sourced from iron corrosion reactions. One such corrosion reaction is from the oxidation of steel, Fe^0 (cr):

$$Fe^0(cr) + 2H_2O \rightleftharpoons Fe^{2+} + H_2 + 2OH^- \text{ Equation 6-10}$$

This transfer of electrons from iron from waste canisters to the brine will be partly responsible for creating the extremely reducing conditions in the repository.

An additional example of corrosion can involve the reduction of iron from electrons donated by sulfide produced from sulfate reduction (Equation 6-11). This reaction also is referred to as steel passivation and can result in increases in gas pressure due to the buildup of H_2 gas.

$$Fe^0(s) + H_2S\ (g) \rightleftharpoons FeS(s) + H_2(g) \quad \text{Equation 6-11}$$

Steel passivation occurrs on the surfaces of the waste canisters that are exposed to gas. Reactions such as Equation 6-11 tend to be limited by the surface area available for reactions and stop when there is no more surface area available for H_2S to corrode.

6.2.3 Actinide Oxidation States

Table 6-1 lists important actinides in the WIPP and their relevant oxidation states in the performance assessment. Because of the predicted reducing conditions in the post closure repository, the PA assumes the reduced forms of Pu—Pu(IV) and Pu(III)—will exist instead of Pu(VI) or Pu(V).

Actinide	WIPP Relevant Oxidation States
U	U(VI), U(IV)
Np	Np(V)
Th	Th(IV)
Pu	Pu(VI), Pu(V), Pu(IV), Pu(III)
Am	Am(III)
Cm	Cm(III)

Table 6-1. WIPP-relevant actinides and oxidation states represented in the PA

Of the reduced Pu species, the PA is uncertain as to which will dominate post-closure and deals with this uncertainty by assuming Pu(III) and Pu(III) solids in 50 percent of model realizations and Pu(IV) and Pu(IV) solids in the other 50 percent. The choice of reduced Pu species is of particular importance because Pu(III) is more soluble than Pu(IV) and can result in higher releases should Pu(III) dominate the post-closure system (Table 6-2).

Solid	Pu Oxidation State	Log K (higher values indicate more soluble solids)	Source
$Pu(OH)_3$	+3	15.8	Lemire et al. (2001)
$Pu(OH)_4$	+4	-0.8	Lemire and Garisto (1989)
PuO_2	+4	-8.03	Lemire et al. (2001)

Table 6-2. Solubility of Pu solid phases.

Multiple redox processes within the repository may affect actinide oxidation state. H_2 generated from steel corrosion (Equations 6-10 and 6-11) can donate electrons to a Pu(IV) solid (e.g., PuO_2 (am)), resulting in its reduction from solid Pu(IV) to aqueous Pu(III). This process also is referred to as reductive dissolution, as demonstrated in Equation 6-12:

$$2PuO_2(am) + H_2 + 6H^+ \rightleftharpoons 2Pu^{3+} + 4H_2O \quad \text{Equation 6-12}$$

Reductive dissolution of a Pu(IV) solid phase may also occur with other electron donors, such as Fe^{2+}, especially if this process is enhanced by the presence of EDTA to stabilize Pu^{3+} that enters into the solution (e.g., Rai et al. 2008). Our current understanding of Pu redox stability is based on calculations using low-ionic-strength systems and data from experimental evidence. Recent data from laboratory experiments suggest that reductive dissolution may occur and may be more important than previously considered (Altmaier et al. 2009, Altmaier and Geckeis 2011, Reed et al. 2011). Furthermore, the contribution of reduced iron solids in the waste containers combined with the high pressure H_2(g) atmosphere created by creep closure will result in extremely reducing conditions that expand the range at

which Pu(III) and Pu(III) solids are stable (Schramke et al. 2020, see Figure 6-2). The red dashed line in Figure 6-2 shows the new range at which Pu species are stable when high repository pressures have been accounted for. This expanded stability especially favors Pu(III) and suggests the need to reassess the current Pu speciation model.

6.3 WIPP-Relevant Oxidizing Reactions

6.3.1 Radiolysis

During radiolysis, molecules (e.g., water) dissociate when they are irradiated by alpha or gamma radiation from radioactive decay (Figure 6-3). Radiolysis produces unstable radicals that will scavenge electrons from reduced species and can contribute to oxidizing conditions.

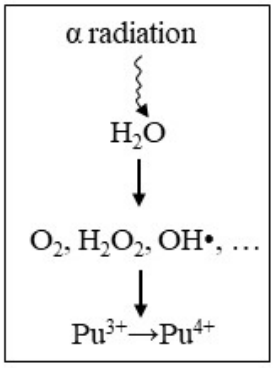

Figure 6-3. Alpha radiation from radioactive decay results in the splitting of H_2O.

$$H_2O + \text{energy} \rightarrow H_2O_2, H_2, \bullet OH, \text{etc.} \quad \text{Equation 6-13}$$

The • refers to an unpaired valence electron that is highly reactive. To reach stability, these unstable compounds steal electrons from other constituents. If a hydroxyl radical encounters ferrous iron, for example, the result is iron oxidation.

$$2\,Fe^{2+} + 2\bullet OH \rightarrow 2Fe^{3+} + 2OH^- \quad \text{Equation 6-14}$$

Hydroxyl radicals will interact further with water to produce hydrogen peroxide (H_2O_2). This substance can decompose into other oxidizing agents as well, such as molecular oxygen.

$$2\,H_2O_2 \rightarrow 2\,H_2O + O_2 \quad \text{Equation 6-15}$$

Hydroxyl radicals also will interact with other components in WIPP brine, producing oxidizing agents like ClO_2, ClO_2^-, ClO_3^-, and ClO_4^-, which all could contribute to an increase in repository E_H.

Radiolysis byproducts also might compete with actinide redox chemistry, such as Pu:

$$2Pu^{3+} + 2\bullet OH \rightarrow 2Pu^{4+} + 2OH^- \quad \text{Equation 6-16}$$

Fortunately, the large amount of steel present in the WIPP likely will interact with the oxidizing agents, acting as a redox buffer to the repository.

Interestingly, one other product of radiolysis is H_2(g), which we showed earlier will create more reducing conditions and increased repository pressures. The extent to which radiolysis will compete with redox processes likely will depend on the actinide inventory at the WIPP.

G-values can be employed to estimate the extent of radiolysis in water. These values, which are measured experimentally, quantify the number of molecules of a byproduct that are produced per 100 eV (electron volts) of absorbed energy. Some examples of G-values are provided in Table 6-3.

G-Value (molecules per 100 eV)							
	H_2	**H**	**e^-**	**H_2O_2**	**OH**	**HO_2**	**H^+**
Alpha radiation	1.4	0.30	0.30	1.3	0.5	0.10	0.3

Table 6-3. Primary products in irradiated water (Day 2019, adapted from Gray 1984)

Similarly, radiolysis will cause the dissociation of complex carbon molecules, such as cellulose from the WIPP CPR. Carbon bonds broken through CPR radiolysis will result in the generation of such gases as carbon monoxide (CO), CO_2, and H_2. Although the quantity of CO produced through this process is likely to be minimal, CO_2 produced can be an issue (see Section 4.3.2).

Initially, DOE screened out the impacts of radiolytic gas generation in the WIPP PA due to its low impact. However, with a significant increase in the Pu inventory (e.g., NAS 2020), the WIPP now considers its impacts to releases. Currently, the WIPP chemistry model assumes the oxidizing effects of radiolysis, and the geochemical implications of CO_2 are negligible as a result of the large amounts of steel and MgO able to buffer the repository. The PA does consider the contribution of radiolytic H_2 on gas pressures, and this will have an effect on repository gas pressure and redox chemistry.

6.3.2 Nitrates

Nitrates (NO_3^-) are present in the waste because of their use in treating actinides. In the redox ladder (Figure 6-1), nitrate is positioned right under O_2, indicating that it is a strong oxidizing agent. Its reaction with organic carbon yields a lot of energy relative to most other electron acceptors below it. The oxidizing nature of nitrate was partly responsible for the 2014 incident that caused a radiation release in the repository. Nitrate in the wastes interacted with the organic absorbent ($C_6H_{10}O_5$) mistakenly used to treat the waste, creating a buildup of CO_2 gas pressure eventually causing a waste canister deflagration (EPA 2017):

$$24\ NO_3^- + 5\ C_6H_{10}O_5 + 24\ H^+ \rightleftharpoons 12\ N_2(g) + 30\ CO_2(g) + 37\ H_2O \quad \text{Equation 6-17}$$

Nitrates in the WIPP will increase the E_H of the system, creating more oxidizing conditions. However, the amount of nitrate relative to other electron acceptors in the waste is negligible, and microorganisms likely will reduce nitrate early in the repository's post-closure history because of the high energy yield produced during its reduction. Removal of the nitrate from the WIPP will allow sulfate reducers to dominate the post-closure microbial metabolic processes.

6.4 The Microbiology of the WIPP

Microbial metabolic processes can profoundly affect the geochemistry of waters and may drive many redox processes in the WIPP. Products from microbial respiration, such as electron shuttles (i.e., organic molecules that can serve as electron carriers in multiple redox reactions), may passively affect the redox chemistry of the repository by altering the movement of electrons, illustrated in Figure 6-4. Furthermore, the mere presence of a microorganism will affect the actinide source term because actinides can sorb onto cell surfaces or accumulate intracellularly, resulting in colloid formation (see Section 7.3).

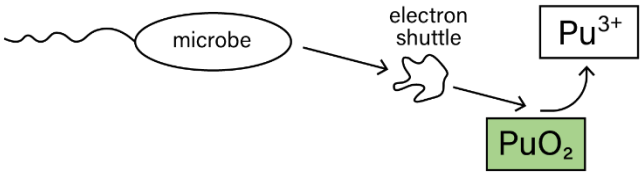

Figure 6-4. Impacts of microbial respiration on Pu oxidation state. Byproducts of microbial respiration, such as electron shuttles, can affect electron flow in the WIPP and reduce Pu

Microorganisms may belong to any one of the three domains of life: *Bacteria*, *Archaea* (e.g., extremophiles found in hot springs), and *Eukarya* (e.g., multicellular organisms like fungi, plants, and animals). Using DNA methods, Swanson et al. (2012) have found all three domains in WIPP brine; the extent of activity of each of these microorganisms in the repository remains uncertain. The extreme salinity of WIPP brine may create thermodynamic constraints to microbial metabolism and viability. In other words, the long-term presence and viability of living microorganisms at the WIPP is highly uncertain and is treated as such in the PA.

Using culturing methods, many different microorganisms or mixed cultures have been isolated from WIPP environments. Two microorganisms in particular, *Chromohalobacter* sp. (Figure 6-5) and *Halobacterium noricense*, an archaeon and bacterium, have been the model organisms used for microbial investigations. Cell counts in the repository have been highly variable and ranged anywhere from 10^4 to 10^7 cells/mL of brine (Swanson et al. 2012). Using these models and a cell count that conservatively bounds the cell counts observed in the repository (10^9 cells/mL), the WIPP calculates both a microbial colloid proportionality constant and maximum value to calculate the microbial contribution to the colloidal actinide source term. This calculation is provided in further detail in Section 7.3.2.

Figure 6-5. Chromohalobacter *sp. isolated from the WIPP; scale bar is at 500 nm*

7 Sorption

Actinides in solution will interact with components in the solution and the surrounding matrix, such as the host rock. These interactions involve the attachment and detachment of actinides on charged surfaces that will facilitate their attachment (sorption). As with other constants examined throughout this document, the amount of actinide sorbed (attached) on a surface can be calculated by using a coefficient, K_d. Sorption is an important part of the WIPP actinide source term because a release into the Culebra will result in actinides' interacting with the host rock, such as the Culebra Dolomite, resulting in their immobilization. Actinides also will sorb onto floating particulates in solutions, such as mineral fragments or microorganisms, forming colloids that enhance actinide mobility.

7.1 Partition Coefficients

A distribution coefficient, K_d, describes the relationship between the amount of a constituent that has been sorbed (adsorbate) onto a surface in relation to the amount of the constituent that remains dissolved in a solution, in cubic meters per kilogram (although the units can vary):

$$K_d\ (\frac{m^3}{kg}) = \frac{Amount\ of\ Solute\ on\ Solid\ Phase\ (\frac{mol}{kg})}{Concentration\ of\ Solute\ in\ Solution\ (\frac{mol}{m^3})} \quad \text{Equation 7-1}$$

Distribution coefficients can also be referred to as partition or retardation or adsorption coefficients. If the solid phase is the host rock, the vast heterogeneity of the subsurface varies greatly, making K_d a fairly site-specific constant. As a result, a K_d value is mostly appropriate for the location at which the constant was measured. Note that, in many cases, sorption of an ion onto a mineral such as clays will include an ion exchange, where the sorption of one ion will result in the release of another. This is not included in the WIPP actinide source term.

Partition coefficients are determined experimentally or in the field. Experimental methods utilize the matrix of interest and measure the amount of sorption that occurs in either a batch experiment or a flowthrough cell. In the field, measurements can be performed using tracers and direct calculations or modeling.

7.2 K_d Values Relevant to WIPP

The Culebra Dolomite is the most transmissive member of the Rustler Formation and could contribute to the spread of actinides during a release to the shallower subsurface beyond the LWA boundary. Therefore, the WIPP PA uses K_d to calculate the amount of actinide that potentially will sorb onto the Culebra and how much will be mobilized. Because K_d values are highly site-specific, using one K_d for the WIPP may not cover the potential range of variability in the dolomite. As such, the PA considers a range of K_d values for the specific actinides of interest, including Pu, Am, U, Th, and Np.

These K_d values all were determined through a series of both batch and flow-through experiments using various matrices ranging from pure dolomite to dolomite-rich Culebra rock to Culebra core samples. The numbers are then fed into PA equations calculating the diffusive flow of brine through the Culebra. The result provides a range of values of the amount of actinide released. Table 7-1 lists the K_d ranges for various actinides calculated in the PA.

7.3 Sorption on Suspended Particles in Solution

Colloids may form as a result of the complexation of actinides with each other to become actinide macromolecules or with such organic macromolecules as humic and fulvic acids (Sections 5.4.2 and 5.4.3). However, colloids also may be formed when actinides sorb onto particles suspended in solutions,

which also provide charged surfaces. The effect of sorption onto colloidal particles, however, is an increased actinide mobilization because their movement through groundwater is based not on diffusion but on Brownian motion (i.e., through the rapid and random collision of colloidal particles with other particles), resulting in a faster dispersal into the environment. In the WIPP, mineral fragments and microorganisms are two colloids that likely will result in actinide sorption.

Actinide	K_d Range [m^3/kg]
Am(III)	0.005–0.4
Pu(III)	0.005–0.4
Th(IV)	0.0005–10
U(IV)	0.0005–10
Np(IV)	0.0005–10
Pu(IV)	0.0005–10
Np(V)	0.00003–0.2

Table 7-1. K_d values for the Culebra Dolomite

7.3.1 Mineral Fragment Colloids

Mineral fragments, or tiny mineral particles suspended in solution, may be actinide macromolecules or may act as sites for actinide sorption. In the WIPP PA, sorption onto mineral fragments was determined through experiments looking at concentrations of actinides that would sorb onto different kinds of mineral fragments, including clays and iron oxides. This quantity was determined by accounting for different factors, including the diameter of the mineral fragment and the number of potential sites available for sorption. Mineral fragment colloid concentrations are added as a supplement to the existing actinide source term and are at a constant value (Papenguth and Behl 1996).

7.3.2 Microbial Colloids

Microorganisms also act as substrates for actinide sorption, although other processes—including bioaccumulation and biomineralization—also will affect the amount of actinide associated with a microorganism. Microbial surfaces contain multiple functional groups with negative charges that could facilitate actinide attachment. In fact, the WIPP microbial colloid proportionality constant (PROPMIC, in mol colloidal actinide per mol dissolved actinide) is calculated in the same manner that a K_d is determined:

$$PROPMIC = \frac{Amount\ of\ Actinide\ Sorbed}{Amount\ of\ Actinide\ Remaining\ in\ Solution} \quad \text{Equation 7-2}$$

Microorganisms are extremely diverse and will have varying degrees of association based on cell type, size, microbial phylotype, and stage in the microorganism life cycle, making the estimation of microbial colloids a very difficult task. The WIPP PA estimates these numbers through experiments using model organisms (see Section 6.4) and the sorption of specific actinides onto these organisms.

8 Criticality

Criticality is a highly unlikely event that may occur at the WIPP if a single nuclear reaction can lead to a chain of subsequent and uncontrolled nuclear reactions, generating a significant amount of heat. Materials at the WIPP capable of causing these chain reactions are referred to as fissile materials and include ^{239}Pu and, to a much lesser extent at WIPP due to minimal inventory, ^{235}U. The addition of significant amounts of Pu into the repository means extra scrutiny will need to be placed on criticality assessments to ensure the safety of the waste.

During a criticality event, a neutron (e.g., from radioactive decay of an actinide) strikes a fissile atom. This causes the nucleus of the neutron-absorbed atom to become unstable and split (fission) into two large fragments, releasing energetic photons (gamma rays) and heating up the surrounding material in the process. This will also result in the release of additional neutrons which in turn will strike other fissile atoms, causing more fissions. Criticality events require a sufficient mass of fissile material assembled into a configuration which will allow for neutrons to strike neighboring atoms in a chain reaction. A critical reaction could then take place, wherein a significant amount of heat is produced very quickly or at worst, a nuclear explosion if this critical mass underwent rapid compression to a high density while chain reactions were occurring and releasing energy.

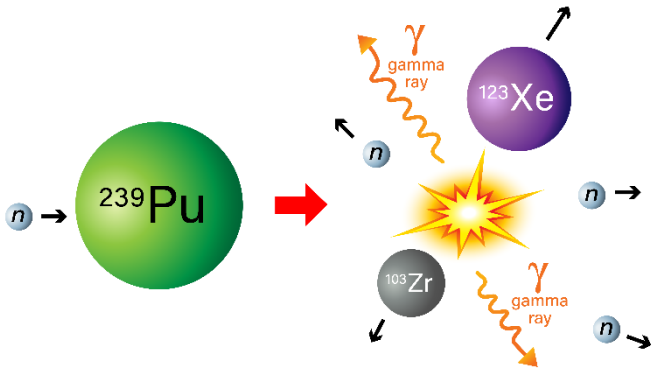

Figure 8-1 Example fission reaction of ^{239}Pu.

An example fission reaction for ^{239}Pu is shown in Figure 8-1 and Equation 8-1 where *n* refers to a neutron, subscripts denote the atomic number (number of protons in the atom), and superscripts denote the mass number (number of protons and neutrons combined).

$$^{1}_{0}n + {}^{239}_{94}Pu \rightarrow {}^{123}_{54}Xe + {}^{103}_{40}Zr + 3{}^{1}_{0}n + energy \quad \text{Equation 8-1}$$

Neutrons generated from the fission of ^{239}Pu can strike neighboring ^{239}Pu atoms in a chain reaction producing increasing amounts of energy in the form of heat (or an explosion if this happens very quickly through a compression, Figure 8-2).

An example fission reaction for ^{235}U is:

$$^{1}_{0}n + {}^{235}_{92}U \rightarrow {}^{236}_{92}U \rightarrow {}^{144}_{56}Ba + {}^{89}_{36}Kr + 3{}^{1}_{0}n + energy \quad \text{Equation 8-2}$$

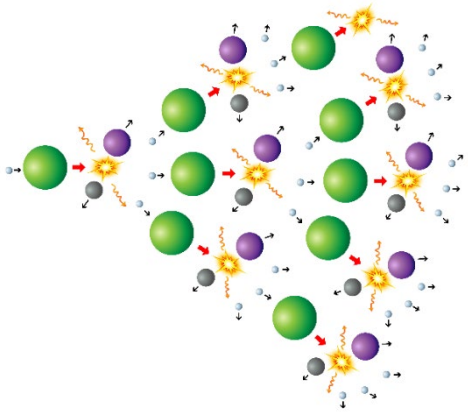

Figure 8-2 Criticality event. A criticality event occurs when a neutron strikes a fissile atom which generates further neutrons that will strike nearby fissile atoms in a chain reaction.

8.1 Factors Impacting Criticality

Neutrons generated from a fissioned atom are fast moving. For a sustained fission reaction to occur efficiently, fast neutrons need to be moderated, or slowed down, so that they can be more easily absorbed by fissile atoms. Water is one example of a neutron moderator which, at the WIPP, would be present as Salado or Castile brine entering the repository.

Besides moderating neutrons, materials may also remove neutrons from the system so that a chain reaction is inhibited. Many neutron poisons are present in the WIPP waste and are sometimes deliberately included to ensure criticality will not occur. Boron is one example of a

neutron poison that can be included in WIPP waste in the form of solid boron carbide. Interestingly, neutron poisons may also be soluble in water and it is notable that a significant amount of boron is already naturally present in WIPP brine.

Should the fissile materials gather in a sufficient mass and configuration, the amount of neutrons available to interact with fissile atoms need to be considered to determine if there is a suitable number of neutrons capable of sustaining a chain reaction. This interaction can be viewed in terms of the ratio of neutrons produced from the current generation of fission compared to the number of neutrons that are lost through absorption and leakage in the previous generation of fission, or k_{eff} (e.g., DOE 1993, Turner 2007):

$$k_{eff} = \frac{neutron\ production\ in\ one\ generation}{neutron\ absorption\ in\ the\ preceeding\ generation + neutron\ leakage\ in\ the\ preceeding\ generation}$$ Equation 8-3

If more neutrons are lost through absorption and leakage than are produced (i.e., $k_{eff}<1$), then a self-sustaining chain reaction cannot occur because there will not be enough neutrons to strike other fissile atoms. Conversely, if the amount neutrons being produced are equal to or greater than the amount of neutrons absorbed or leaked, then a chain reaction can occur and criticality is possible. Criticality assessments examine the changes in k_{eff} with different configurations of waste canisters placed in panels as well as with the presence or absence of various materials that may act as neutron poisons.

8.2 Criticality at the WIPP

Criticality at the WIPP is evaluated in the FEPs under the category of Nuclear Criticality: Heat and Nuclear Explosions (e.g., DOE 2019c). For criticality to occur at the WIPP, fissile materials in the waste need to be sufficiently assembled into a critical mass and a geometry such that a sustainable reaction can occur. The mechanisms that have been identified that could cause this include geochemical (solubility, sorption, precipitation) and mechanical (compaction) or a combination of both. However, various analyses and models indicate that these processes are highly unlikely to get k_{eff} to 1 or greater.

8.2.1 Geochemical Constraints to Criticality

Models to determine criticality involve looking at the mass and shape of fissile materials at the WIPP in the presence of Castile or Salado brine as a moderator. For simplicity, models examine a range of ^{239}Pu spheres of different radii and masses in the presence of brine with varied dissolved ^{239}Pu concentrations and minerals present (e.g., Rechard and Sanchez 2019). Model results indicate that even the maximum dissolved Pu(III) concentration in brines at WIPP is still three orders of magnitude below the limits necessary to create a critical solution. A similar conclusion was also reached with ^{235}U.

Still, DOE explored what possibilities may occur to concentrate radionuclides such that a critical solution could be created (e.g., Rechard and Stein 2019). One geochemical mechanism identified is the solubilization of the fissile actinides. However, both Pu and U do not have a high enough solubility in WIPP conditions to concentrate the metals into criticality. Similarly, colloids may also present another possibility of actinide concentration whereby colloidal particles may concentrate and settle (see Sections 5.4, 7.3.1, and 7.3.2). However, calculated colloidal concentrations are still several orders of magnitude below the lower limit needed to induce criticality. Moreover, colloidal agglomeration would likely be uniform throughout the repository, making it unlikely for masses of colloidal ^{239}Pu or ^{235}U to settle.

Another mechanism potentially concentrating fissile actinides is sorption (see Section 7). Potential sorptive sites in the waste disposal area include the waste canisters as well as waste components such as soils, clays, corroded metals, and degraded glass. However, these materials are diffuse in the repository, making concentration of ^{239}Pu or other fissile actinides unlikely.

Precipitation may also occur that could bring actinides out of solution and concentrate them. However, the geochemistry of the disposal area is fairly uniform and is moderated by Fe redox chemistry (see

Section 6). For precipitation to occur appreciably, localized changes would have to occur within the WIPP brine which would cause significant amounts of precipitation of fissile actinide. Although possible, this is also inconsistent with the conceptual model of WIPP brine being a homogeneous solution.

These same conditions also apply to dissolved and colloidal fissile materials in the repository in the event of an inadvertent intrusion. Brine flowing up a borehole will likely filter and concentrate fissile actinides into localized microenvironments. The boreholes themselves will not have diameters large enough to support the radius and mass of fissile material capable of causing a criticality event. In the far field environment (i.e., the Culebra, see Section 10.3.2), although changes will occur with redox chemistry and salinity as brine enters the Culebra, conditions do not favor precipitation into appreciable amounts as the increase in oxidation will likely increase solubility (though not into amounts that can be of concern). The concentration of sorptive sites is low and will not cause the concentration of actinides that can result in a criticality event. Furthermore, the Culebra is composed of centimeter-sized microenvironments of poorly connected pores that are not conducive to concentrating fissile materials.

8.2.2 Geomechanical Constraints to Criticality

Compression, especially from rock falls and salt creep, may also enhance the likelihood of fissile material from waste emplaced in a favorable geometric configuration to undergo a criticality event. DOE has performed multiple simulations at different timepoints in the repository 10,000-year timeframe, with different combinations of brine intrusion, gas generation, salt creep, and rock fall geometries (e.g., Rechard 2019, Saylor and Scaglione 2018) and show that the possibility of criticality or explosions appears unlikely (Figure 8-3).

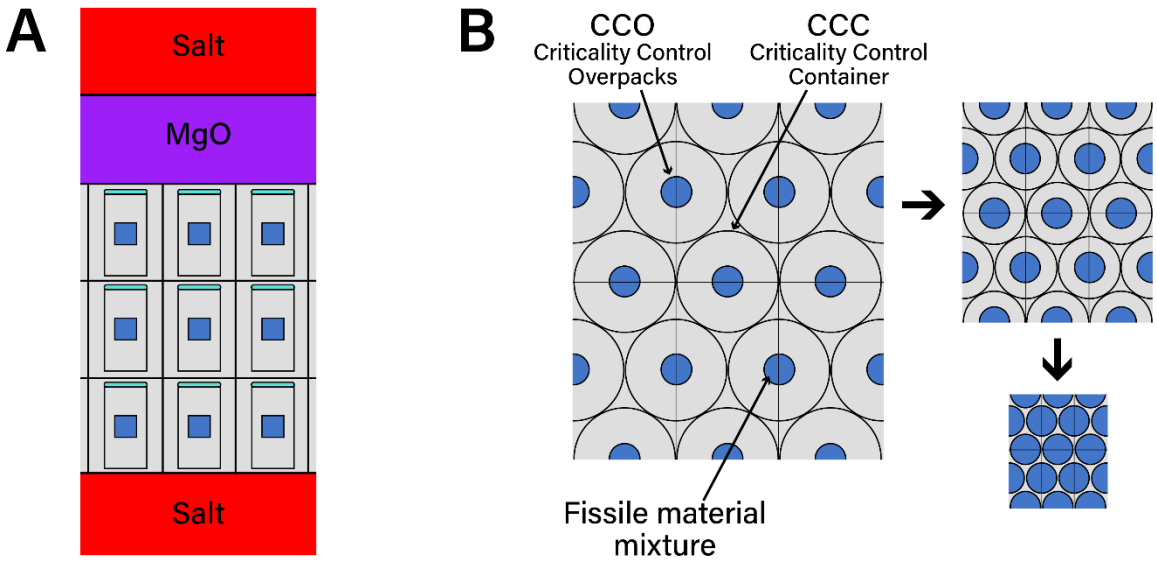

Figure 8-3 DOE simulations for criticality. Simulations of criticality at the WIPP look at changes to k_{eff} based on various configurations of waste containers containing fissile materials in the repository as well as their compression; A) side view of simulated stacked waste containers, B) top view of simulated waste containers (adapted from Saylor and Scaglione 2018).

The containers shown in Figure 8-3 represent criticality control containers (CCC) inside criticality control overpacks (CCO), which is one method of storing Pu into waste canisters. In this case, the CCCs are cylinders with a diameter of 16.8 cm and a height of 68.4 cm which contain up to 300 fissile gram equivalents of Pu. These CCCs are then stored in CCOs which have a diameter of 57.5 cm and a height of 88.3 cm. Although these containers will be compressed during salt creep, models indicate that a configuration promoting criticality cannot be reached and that contents of the containers themselves will

also absorb neutrons. Wastes may also contain further additives such as neutron poisons so that stray neutrons from fission cannot trigger a criticality event.

9 Geochemical Modeling

Although it is possible to calculate solubilities, saturation indices, and geochemical speciation by hand, waters with more dissolved solids will have multiple ion interactions occurring, making calculations difficult and tedious. Geochemical modeling programs simplify this task and perform a multitude of reactions, including acid-base, complexation, dissolution and precipitation, redox, sorption, and gas chemistry. Programs also can couple geochemical calculations with physical models of advection, dispersion, and transport. Actinide solubility is estimated through geochemical modeling at the WIPP.

Underlying many geochemical models is the assumption of equilibrium, although disequilibrium can be modeled by adjusting input parameters. Although the reality is that most reactions in real life do not reach equilibrium, providing calculations at equilibrium gives useful insights into a system. Models, for example, provide information about what minerals are favored to dissolve or precipitate and the distribution and speciation of important metals in the water.

Geochemical Codes

Multiple geochemical codes exist to perform modeling, and three examples are highlighted below.

EQ3/6 (Wolery 1992) is the primary code being used for the WIPP PA. This program uses EQ3 for geochemical speciation with EQ6 for reaction path calculations (e.g., water-mineral interactions). The program is publicly available, although the database used to model WIPP actinides has been tailored specifically for the repository. The database also can model kinetics and provides calculations from a starting point until a water reaches equilibrium.

PHREEQC (Parkhurst and Appello 1999) is a publicly available program produced by the U.S. Geological Survey. In addition to speciation and reaction path calculations, the program also can perform inverse models, which simulate the evolution of a water from multiple endmember waters. The program also can perform one-dimensional reaction transport modeling.

Geochemist's Workbench (Bethke 1994) is a collection of five geochemical programs and can perform reactive transport, inverse modeling, and graphical output. The program is commercially available.

Box 9-1. Geochemical codes

9.1 Modeling

9.1.1 Databases

Geochemical modeling programs utilize databases, which provide the useful information needed to make the calculations. Databases comprise multiple components:

- *Basis species:* These "building blocks" are the minimum chemical formulas needed to describe the composition of the solution. These also can be referred to as "component species" or "master species."

- *Secondary species:* These are species that build off a basis species (e.g., redox species or complexes). For example, Pu can exist in multiple redox states in a solution. The basis species for Pu may be Pu^{6+}, although it also may exist as Pu^{5+}, Pu^{4+}, Pu^{3+}, as well as various aqueous complexes that are included as secondary species. The database then provides the relationship of the Pu species to one another, such as through redox equations (e.g., $Pu^{5+} = Pu^{6+} + e^{-}$). This relationship also includes equilibrium constants that relate the different species to the basis.

- *Minerals:* As with secondary species, minerals are solid phases in the database and are described using the basis species and an equilibrium constant.

- *Gases:* Gaseous species also are described in terms of the basis species and equilibrium constants.

- *Sorption and exchange:* Some databases will provide sorption information, so users can calculate interactions of ions with surfaces.

- *Aqueous model:* Databases also may contain relevant data to perform chemical speciation using a specific model of ion interactions. This could include Pitzer parameters or SIT coefficients. Most model codes provide the option to perform calculations using different ion interaction models because the databases used in the calculations provide the necessary data.

Waters, such as WIPP brine, are very complex solutions with multiple ions interacting with one another. Creating a database is a long, difficult process that requires selecting the most appropriate equilibrium constants and parameters that best represent the system being modeled. To ensure the right data are included and that ions interact the way they are intended to, good databases also are tested against real-world systems to demonstrate their effectiveness in modeling reality.

```
     3 element(s):
      3.0000 H              4.0000 O              1.0000 P
****
     3 species in aqueous dissociation reaction:
    -1.0000  H3PO4(aq)                 2.0000  H+
     1.0000  HPO4--
*
**** logK grid [0-25-60-100C @1.0132bar; 150-200-250-300C @Psat-
H2O]:
        No_Data   -9.3517   No_Data   No_Data
        No_Data   No_Data   No_Data   No_Data
* Source:
+----------------------------------------------------------------
H2PO4-                     H2PO4-
     charge  =  -1.0
****
     3 element(s):
      2.0000 H              4.0000 O              1.0000 P
****
     3 species in aqueous dissociation reaction:
    -1.0000  H2PO4-                    1.0000  H+
     1.0000  HPO4--
*
**** logK grid [0-25-60-100C @1.0132bar; 150-200-250-300C @Psat-
H2O]:
        No_Data   -7.2062   No_Data   No_Data
        No_Data   No_Data   No_Data   No_Data
* Source:
+----------------------------------------------------------------
PO4---                     PO4---
     charge  =  -3.0
****
     2 element(s):
      4.0000 O              1.0000 P
****
     3 species in aqueous dissociation reaction:
    -1.0000  PO4---                    -1.0000  H+
     1.0000  HPO4--
*
**** logK grid [0-25-60-100C @1.0132bar; 150-200-250-300C @Psat-
```

Figure 9-1. The FMT database used for the WIPP

9.1.2 Model Inputs and Outputs

Input files to models usually provide the program with information on the water being modeled, such as basis species (i.e., initial water composition), pH, temperature, units of measure, and minerals and gas phases to equilibrate with the water. After the model has performed its calculations, output files often can provide volumes of information, including solution pH, speciation of different constituents, concentrations and activities of components in solution, concentrations and activities of complexes present, and mineral saturation indices.

9.1.3 Model Uncertainties

Model outputs need to be examined with a critical eye. Reaction outputs may be intricate and may present data that are thermodynamically possible but not observed in the real world. For example, output files may suggest dolomite or feldspar precipitation, two processes that have not been observed in low-temperature systems in the real world. Additionally, models also may

Thermodynamic Data Selection

Multiple resources are available to compare and potentially select thermodynamic data for use in geochemical modeling. For low ionic strength systems, the Nuclear Energy Agency (NEA) Thermochemical Database (TDB) (Ragoussi and Brassinnes 2015, Martinez et al. 2019) provides an internationally recognized, internally consistent database that contains formation and reaction data for aqueous solid and gaseous elements, calculated from a thorough review of the literature and an expert selection of experimental values and calculations. Data selection is documented fully in the NEA's TDB volumes. Andra's ThermoChimie (Griffaut et al. 2014) and the Japan Atomic Energy Agency (Kitamura et al. 2010) also have databases that utilize similar selection criteria as the NEA but have expanded them to include aqueous species excluded by the NEA.

The Thermodynamic Reference Database (THEREDA) (Altmaier 2011) also provides useful formation and reaction data, as well as Pitzer parameters for higher–ionic strength systems. The database project utilizes a similar model for data selection as the NEA but has expanded its criteria to include high-ionic-strength media.

Box 9-2. Thermodynamic data selection

have multiple limitations, and such topics as kinetics, redox equilibria, and chemical heterogeneity of a system may not be adequately addressed because many model databases do not contain enough data to be able to address these topics.

Thermodynamic values used in models all rely on measured or estimated data, which all have a degree of uncertainty. These uncertainties will be propagated through a model calculation, resulting in imprecision in such calculations as saturation index, pH, and so on. Thermodynamic values chosen in model databases also may be chosen from multiple sources, resulting in inconsistencies in the database and added uncertainties. Determining an internally consistent database is a large task and requires a degree of technical judgement.

```
|-------------------------------------------------------------------------------|
|Aqueous Basis Species/Constraint Species        |Conc., etc. |Units/Constraint|
|  (uspeci(n)/ucospi(n))                         | (covali(n))|(ujf3(jflgi(n)))|
|-------------------------------------------------------------------------------|
|Na+                                             | 3.53000E+00|Molarity        |
|K+                                              | 4.67000E-01|Molarity        |
|Mg++                                            | 1.02000E+00|Molarity        |
|Ca++                                            | 1.40000E-02|Molarity        |
|Cl-                                             | 5.86000E+00|Molarity        |
|HCO3-                                           | 1.60000E-02|Molarity        |
|SO4--                                           | 1.77000E-01|Molarity        |
|B(OH)4-                                         | 1.58000E-01|Molarity        |
|Br-                                             | 2.66000E-02|Molarity        |
|H+                                              | 6.00000E+00|pH              |
|NpO2+                                           | 1.00000E-18|Hetero. equil.  |
|->|KNpO2CO3                                     |  (ucospi(n))   |
|Th++++                                          | 0.00000E+00|Hetero. equil.  |
|->|ThO2(am)                                     |  (ucospi(n))   |
|Am+++                                           | 1.00000E-18|Hetero. equil.  |
|->|Am(OH)3(s)                                   |  (ucospi(n))   |
|Acetate-                                        | 2.83000E-02|Molarity        |
|Citrate---                                      | 2.30000E-03|Molarity        |
|EDTA----                                        | 7.92000E-05|Molarity        |
|Oxalate--                                       | 1.13000E-02|Molarity        |
|Pb++                                            | 1.00000E-18|Molarity        |
|Fe++                                            | 1.00000E-18|Molarity        |
|-------------------------------------------------------------------------------|
* Valid jflag strings (ujf3(jflgi(n))) are:                                    *
*    Suppressed          Molality            Molarity                          *
*    mg/L                mg/kg.sol           Alk., eq/kg.H2O                   *
*    Alk., eq/L          Alk., eq/kg.sol     Alk., mg/L CaCO3                  *
*    Alk., mg/L HCO3-    Log activity        Log act combo                     *
*    Log mean act        pX                  pH                                *
*    pHCl                Hetero. equil.      Homo. equil.                      *
*    Make non-basis                                                            *
*-------------------------------------------------------------------------------*
|Create Ion Exchangers  | (net)                                                 |
|-------------------------------------------------------------------------------|
|Advisory: no exchanger creation blocks follow on this file.                    |
|Option: on further processing (writing a PICKUP file or running XCON3 on the   |
|present file), force the inclusion of at least one such block (qgexsh):        |
|  [ ] (.true.)                                                                 |
|-------------------------------------------------------------------------------|
```

Figure 9-2. Example input file for EQ3/6

WIPP Actinide Uncertainty Distribution

The WIPP utilizes a unique approach to address uncertainties during geochemical modeling that arise from a variety of factors, such as experimental uncertainties from the thermodynamic values chosen for model databases. This uncertainty approach also is utilized because the final repository conditions are not completely known and may fall within a range of possibilities.

Actinide geochemical uncertainty is addressed by comparing experimental values to modeled values of that same experiment. These values are placed in a distribution that subsequently is randomly sampled. Values chosen from this distribution are used to adjust the values calculated during the performance assessment. Experiments that are chosen to model for this uncertainty distribution are chosen from the literature and are selected based on multiple criteria points, including how relevant the studies are to WIPP brine. Specifically, the uncertainty distribution looks at the differences (D) between the logarithms of the molar experimental values (log S_m) and modeled values (log S_p) for the +3 or the +4 actinides.

$$D = \log S_m - \log S_p$$

Positive D values show larger experimental values relative to modeled values and indicate that PA calculations underpredict actinide solubility. Conversely, negative D values indicate that model values are larger than experimental values, suggesting that PA calculations overpredict solubilities.

The graphs below represent the uncertainty distributions for +3 (left) and +4 actinides (right) for the 2014-CRA and the EPA-mandated 2014-CRA SEN4 sensitivity study. The *y*-axis cumulative probability represents the different experiments chosen for the uncertainty distribution, whereas the *x*-axis represents the D values for each distribution. The values compare the uncertainty distribution used for the 2014 performance assessment (black line) in comparison to a sensitivity study (red line) using a different set of criteria for selecting experiments. The location of the black curve relative to the red curve in the +3 actinides suggest that the 2014-CRA underpredicted solubilities relative to the SEN4 study. For +4 actinides, the 2014-CRA slightly overpredicted solubilities relative to SEN4.

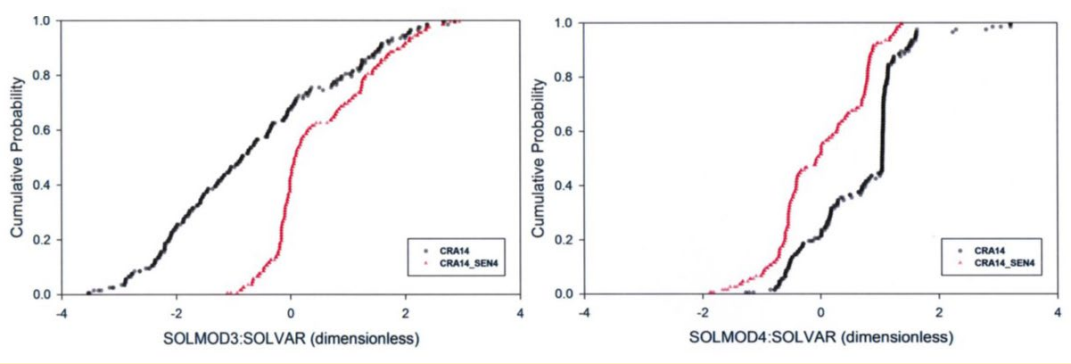

Box 9-3. WIPP actinide uncertainty distribution

10 Performance Assessment

The WIPP performance assessment uses a series of computer simulations to provide an analysis that estimates the potential cumulative release of radionuclides over the 10,000-year regulatory period. In addition to including all of the geochemical concepts outlined in the previous chapters as part of the chemical conceptual model, it also accounts for other physical processes, such as fluid flow, and their impact on the repository's performance.

The PA includes methodology that identifies the features, events, and processes (FEPs) that could affect repository performance and contribute to a release. It also evaluates repository performance in both undisturbed and disturbed scenarios. Of the various scenarios identified in the FEPs, only disturbances related to oil and gas drilling result in significant releases.

The PA consists of a large number of calculations (3 replicates of 100 separate calculations) carried out using sets of sampled parameter values. Results of disturbed repository calculations are represented in horsetail plots (Figure 10-1) that describe the magnitude of the release in EPA units (see Box 10-1) across a range of probabilities. The horsetail plot in Figure 10-1 provides the results of 300 sets of calculations for the PA in CRA-2014.

EPA Units

The WIPP PA calculates releases in terms of EPA units, which is a unit of activity normalized toward its release limit. To calculate EPA units, a waste unit factor (WUF) is first calculated. The WUF allows the WIPP to pay specific attention to the long-lived, alpha-emitting radionuclides in the number of millions of curies (Ci). It also allows us to pay attention to the wastes most important over the repository's 10,000-year performance.

$$WUF = \frac{\sum_i W_i}{10^6 Ci}$$

$\mathbf{W_i}$ is the activity in Ci at closure for the alpha-emitting TRU repository wastes at WIPP that have half-lives greater than 20 years.

Using the WUF, an EPA unit then can be calculated:

$$\boldsymbol{E_i = \frac{w_i(t)}{WUF \times r_i}}$$

where:

$\mathbf{E}_i$ are the EPA units.

$\mathbf{w_i(t)}$ is the activity for radionuclide *i* at time *t*.

$\mathbf{r_i}$ is the release limit of radionuclide *i* as dictated by 40 CFR Part 191.

Box 10-1. EPA Units.

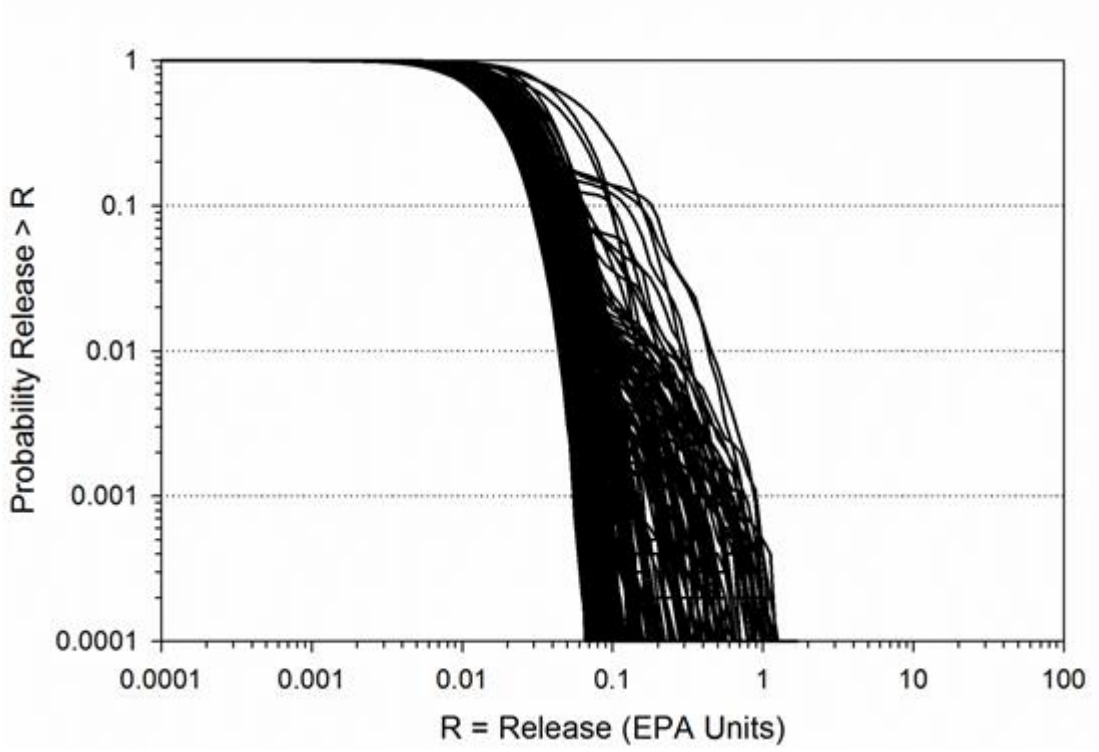

Figure 10-1. Horesetail plot of releases from CRA-2014 (DOE 2014b)

10.1 Undisturbed Repository

In an undisturbed repository, the surrounding Salado Formation is expected to encapsulate the waste. Specifically, because of the ductile nature of salt under pressures experienced at the waste horizon, we expect to see the formation creep, heal, and decrease in porosity. Multiple geochemical processes also are expected to occur, including the generation of gas from iron corrosion, microbial respiration, and radiolysis. Formation brine will enter the repository and dissolve some actinides in the waste. Some of this brine also could be released from the repository through fractures in the anhydrite and clay interbeds in the Salado; however, calculations show that the amount that potentially could reach the surface will be negligible.

10.2 Disturbed Repository

Because of the abundance of oil and gas in the Delaware Basin, the WIPP PA calculates the potential of a release from an accidental intrusion resulting from drilling (Figure 10-2). When an intrusion through drilling occurs, multiple routes for a potential release are possible, including cuttings and cavings, spallings, DBR, and long-term brine releases to the Rustler Formation or to the surface.

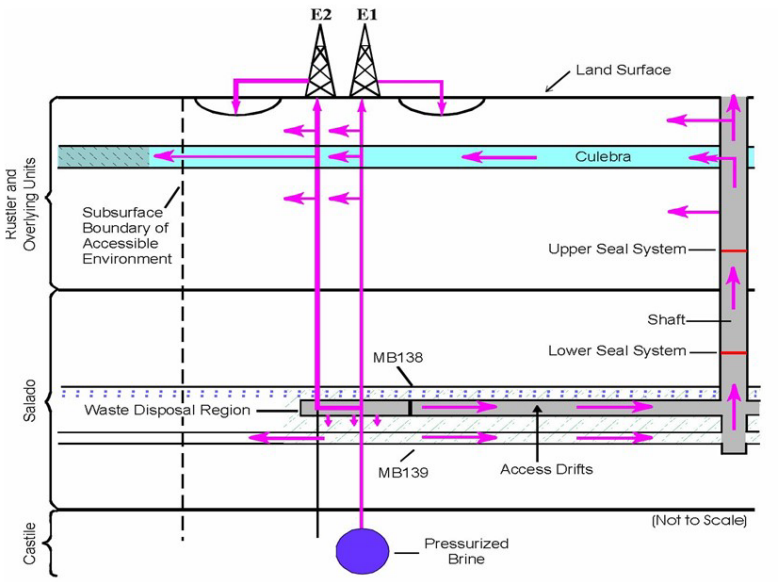

Figure 10-2. Schematic of a direct brine release

10.2.1 Cuttings and Cavings

Cuttings refer to the volume of material brought to the surface as a result of drilling. The quantity of radionuclides released is a function of the activity of the waste that was drilled into and the diameter of the intruding drill bit. Different waste streams will have different activities, and the PA considers random penetrations during its calculations.

Cavings are the particulate material eroded from a borehole wall by the drilling fluids. Drilling mud from the drilling activity will flow up a borehole and apply a stress to the borehole walls. At high enough stresses, erosion of the wall materials can occur and bring radionuclides up to the surface. Calculations of cavings rely on multiple factors, including the diameter of the drill bit, the resistance of the intruded material, and the speed and viscosity of the drill bit.

10.2.2 Spallings

Spallings releases also are related to drilling. However, unlike cuttings and cavings, spallings rely on pressure and occur if the gas pressure in the repository is high enough (> 100 atm) to push additional waste material up a borehole. The volume of spallings pushed up a borehole will depend on the physical properties of the material that was drilled.

10.2.3 Direct Brine Release (DBR)

During a DBR, brine from the Salado first infiltrates the repository and interacts with the waste. This brine also may come from a previous drilling intrusion that encounters a brine pocket in the Castile below the repository and fills the repository with pressurized brine. When subsequent drilling occurs, mobile brine in the repository enters the borehole and flows to the surface. As with spallings, DBRs require repository pressures to reach a threshold pressure (> 80 atm) for brine to be pushed up the borehole and onto the surface. This occurrence, although a low probability event, relies on the understanding of the repository geochemistry because actinides will migrate in brine as dissolved and colloidal species. The concepts outlined in this document relate most directly to this form of release.

10.2.4 Culebra Flow

In the event of a long-term brine release up an abandoned borehole, the Culebra likely is the unit that will facilitate actinide dispersal because it is the most transmissive unit above the Salado. Calculations of actinide releases rely on both advective and diffusive flow through the Culebra's fractures and vugs.

10.3 Estimation of Releases

10.3.1 Source Term Calculation

The total mobile actinide concentration in brine is calculated as the sum of the dissolved and colloidal actinide source terms (i.e., for each of the realizations calculated for PA based on the sampled parameters):

$$\text{Total Mobile Actinides} = \text{Dissolved Actinides} + \text{Humic Colloids} + \text{Intrinsic Colloids} + \text{Mineral Fragment Colloids} + \text{Microbial Colloids}$$

10.3.1.1 Dissolved Actinides

The dissolved actinide concentration is calculated using the log K values and Pitzer parameters of actinides in WIPP brine as modeled in the geochemical database. This value is adjusted to account for uncertainty in parameter values and in repository conditions by using a value from the uncertainty distribution.

$$\text{Dissolved actinide concentration} = \text{Baseline Solubility} \times 10^{(\text{sampled value from uncertainty distribution})}$$

10.3.1.2 Colloids

Four types of colloids can form in the WIPP: mineral fragment (Section 7.3.1), intrinsic (Section 5.4.3), microbial (Section 7.3.2), and humic (Section 5.4.2). The WIPP PA calculates these values and adds them to the dissolved actinide source term. This results in the total actinide source term. Both intrinsic and mineral fragment colloids are constant values that are derived experimentally. That is—

Mineral Fragment Colloid = Constant Value from experiments

Intrinsic Colloid = Constant Value from experiments

Humic and microbial colloids are calculated from experimentally derived proportionality constants. These are multiplied by the dissolved actinide concentration to obtain a number that adds to the dissolved actinide source term calculation:

Microbial Colloid = Dissolved × Microbial Colloid Proportionality Constant

Humic Colloid = Dissolved Actinide × Humic Colloid Proportionality Constant

If humic or microbial colloid concentrations reach an upper limit, that value is replaced by an upper-bound value that also is experimentally derived.

10.3.1.3 Oxidation States

Solubility calculations are performed using Am(III) to represent the +3 actinides, Th(IV) to represent the +4 actinides, and Np(V) to represent +5 actinides. U(VI) is the only +6 actinide and is set to a constant value. For actinides with multiple oxidation states, such as Pu, the PA uses the +3 actinides for 50 percent of realizations and +4 actinides for the other 50%. This distribution initially was chosen because of a lack of information on Pu behavior and an unclear picture of the repository conditions post-closure. However, data now suggest that Pu(III) will provide a larger contribution to the dissolved actinide source term than Pu(IV) (e.g., Schramke et al. 2020).

10.3.2 Transport Through the Culebra

The Culebra can be characterized as a double-porosity medium, with its porosity consisting of interconnected fractures and vugs (cavities). Models of actinide transport through this medium are derived from laboratory and field investigations that examine the physical processes of transport through the Culebra and the behavior of dissolved and colloidal actinides.

Actinide transport in the Culebra is affected by multiple mechanisms. First, transport is slowed by physical retardation, wherein actinides will diffuse into and back out of the porosity of the Culebra. Second, actinides will be slowed through chemical retardation during interactions with the dolomite, during which actinides will sorb onto the dolomite grains of the matrix. This is calculated by applying K_d values to diffusive transport.

10.4 Performance Assessment Calculation

DOE performs three replicates of 100 separate calculations in the PA. Each of these 100 calculations contains sets of parameter values related to the conditions in and around the repository and related to future human intrusions.

Each calculation includes 10,000 sets of potential futures that are a representation of a series of human intrusion events. The total mobile actinide source term estimates a radionuclide release as a function of a possible future. The PA calculation uses a probabilistic approach, providing the results of multiple possible outcomes over a range of probabilities.

To perform this calculation, the PA first samples 63 uncertain parameters (via Latin Hypercube sampling, a method to perform random sampling using a set of parameters) related to the conditions in and around the repository and future events. Subsequently, 10,000 futures are constructed by incorporating the drilling rates around the Delaware Basin and the probabilities of—

- intrusion into an excavated area.
- drilling into a brine pocket.
- penetrating RH or CH waste.

Each future result is a cumulative release with equal probability. The results of these futures are sorted from smallest releases to largest releases and plotted into a complementary cumulative distribution function (CCDF, Figure 10-1). Because a total of 300 vectors are used in the analysis and 10,000 futures are constructed for each vector, the number of potential futures simulated in the PA is 3 million. The process for generating a future is as follows:

1. Begin with the time of intrusion (if there is an intrusion).
2. Determine the frequency of the intrusion (i.e., if it is a one-time intrusion or if multiple intrusions occur in the repository).
3. Define the borehole intrusion (i.e., where in the repository—if at all—the intrusion occurs).
4. Calculate spallings, cuttings, and DBRs.
5. Repeat steps 1 through 4 until 10,000 futures have been calculated.
6. Calculate flows through the Culebra across all events.
7. Create output CCDF plots.

The average of all of the different vectors then can be used to demonstrate compliance when the values fall below EPA release limits. Figure 9-3 provides the average releases from the horsetail plot in Figure 10-1. It demonstrates two sets of calculations, one used during the 2014-CRA and another from the EPA mandated SEN4 sensitivity study, which adjusted several parameter inputs to the PA. Both curves demonstrate a range of probabilities, as well as cumulative releases. Although the total releases differ slightly, both fall well below the release limits at 0.1 probability and 1 EPA unit and at 0.001 probability and 10 EPA units ([0.1, 1] and 0.001, 10]) and shown in the figure.

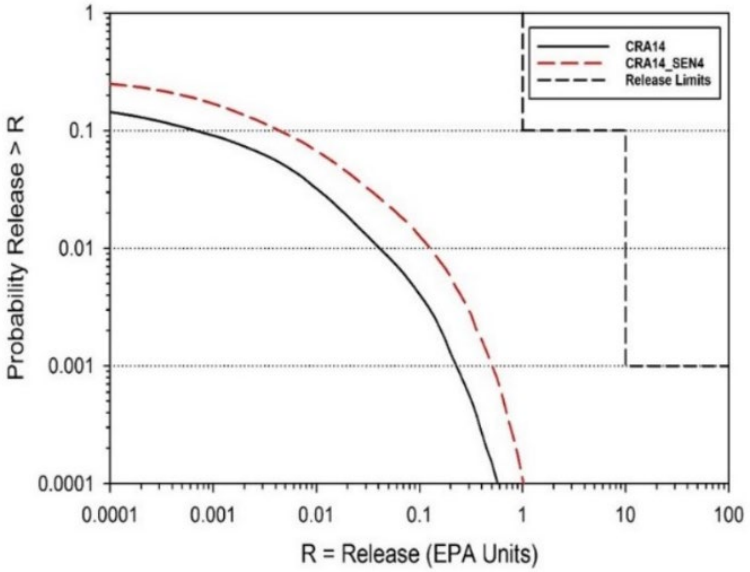

Figure 10-3. Performance assessment results for a DBR for CRA-2014

11 Acronyms, Abbreviations and Initialisms

(am)	amorphous
(aq)	aqueous
(cr)	crystalline
(g)	gaseous
(s)	solid
β	stability constant
^{144}Ba	barium with a mass number of 144
^{89}Kr	krypton with a mass number of 89
^{239}Pu	plutonium with a mass number of 239
^{235}U	uranium with a mass number of 235
^{236}U	uranium with a mass number of 236
^{103}Xe	xenon with a mass number of 103
^{123}Xe	xenon with a mass number of 123
^{103}Zr	zircon with a mass number of 123
a_H	ion activity
Am	americium
Am^{3+}	americium cation in the +3 oxidation state
$AmCl^{2+}$	americium chloride ion – (1:1) complex
$AmCl_2^{+}$	americium chloride ion – (1:2) complex
$Am(OH)_3$	americium hydroxide
atm	atmosphere
$B(OH)_3$	borate
$B(OH)_4^{-}$	hydroxyborate ion – (1:4) complex
Ca^{2+}	calcium cation
$C_2H_3O_2^{-}$	acetate
$C_2O_4^{2-}$	oxalate
$C_6H_8O_7$	citrate
$C_6H_{10}O_5$	cellulose
$C_{10}H_{16}N_2O_8^{4-}$	ethylenediaminetetraacetic acid
$CaCO_3$	calcite
$CaCO_3.6H_2O$	ikaite
$CaCO_3.H_2O$	monohydrocalcite
$CaMg(CO_3)_2$	dolomite
$Ca(OH)_2$	cementitious material, portlandite
$CaSO_4$	anhydrite
CCA	compliance certification application
CCC	criticality control container
CCDF	complimentary cumulative distribution function
CCO	criticality control overpack
CH	contact handled
CH_4	methane
Ci	curie
CID	Comprehensive Inventory Database
Cl^{-}	chloride anion
ClO_2	chlorine dioxide
ClO_2^{-}	chlorine dioxide anion
ClO_3^{-}	chlorate anion
ClO_4^{-}	perchlorate anion

Cm	curium
CO	carbon monoxide
CO_2	carbon dioxide
CO_3^{2-}	carbonate
CPR	cellulosics, plastics, and rubber
CRA	compliance recertification application
DBR	direct brine release
DOE	U.S. Department of Energy
EDTA	ethylenediaminetetraacetic acid
E_H	redox potential
EPA	U.S. Environmental Protection Agency
EQ3/6	DOE software program for geochemical modeling of aqueous system
ERDA-6	Energy Research and Development Administration Well 6
e^-	electron
eV	electron volt
Fe	iron
Fe^0	zero-valent iron, steel
Fe^{2+}	aqueous ferrous iron
Fe^{3+}	aqueous ferric iron
$Fe(OH)_3$	ferrihydrite
FEPs	features, events, and processes
FeS	iron sulfide
FMT	Fracture-Matrix Transport code
GWB	Generic Weep Brine
H^+	hydrogen ion
H_2	hydrogen
H_2CO_3	carbonic acid
H_2O_2	hydrogen peroxide
H_2S	hydrogen sulfide
HCO_3^-	bicarbonate
Hs	humic acid
K	solubility constant
K^+	potassium cation
$K_2MgCa_2(SO_4)_4•2H_2O$	polyhalite
KCl	sylvite
K_d	distribution coefficient
k_{eff}	ratio of neutrons produced from the current generation of fission compared to the number of neutrons that are lost through absorption and leakage in the previous generation of fission
kg	kilogram
K_H	Henry's Law constant
K_{sp}	solubility product
LWA	Land Withdrawal Act
m	molal
M	molar
MB	Marker Bed
mg/L	milligrams per liter
Mg^{2+}	magnesium cation
$MgCl_2$	magnesium chloride
$MgCO_3$	magnesite
$MgCO_3•3H_2O$	nesquehonite

$Mg_2Cl(OH)_3 \cdot 4H_2O$	phase 3
$Mg_3(OH)_5Cl \cdot 4H_2O$	phase 5
$Mg_4(CO_3)_3(OH)_2 \cdot 3H_2O$	hydromagnesite4323
$Mg_5(CO_3)_4(OH)_2 \cdot 4H_2O$	hydromagnesite (hydromagnesite5424)
MgO	magnesium oxide, periclase
$Mg(OH)_2$	brucite
mL	milliliter
mol/kg	moles per kilogram
mol/L	moles per liter
mrem	millirem
n	neutron
Na^+	sodium cation
$Na_2B_4O_7 \cdot 10H_2O$	borax
NaCl	halite
NEA	Nuclear Energy Agency
NO_3^-	nitrates
Np	neptunium
NpO_2^+	neptunyl cation
NpO_2OH	neptunium (V) hydroxide
$NpO_2(OH)_2^-$	neptunium (V) hydroxide ion – (1:2) complex
Np(V)	neptunium in the +5 oxidation state
O_2	oxygen
OH^-	hydroxide
PA	Performance Assessment
PAIR	Performance Assessment Inventory Report
p_cH	negative logarithm of hydrogen ion concentration in moles per liter
pe	negative logarithm of electron activity
pH	negative logarithm of hydrogen ion activity
PHREEQC	U.S. Geological Survey software program for geochemical modeling of aqueous systems
p_mH	negative logarithm of hydrogen ion concentration in moles per kilogram
PROPMIC	proportionality constant describing microbial bioassociation with actinides
Pu	plutonium
Pu^{3+}	plutonium cation in the +3 oxidation state
Pu^{4+}	plutonium cation in the +4 oxidation state
Pu^{5+}	plutonium cation in the +5 oxidation state
Pu^{6+}	plutonium cation in the +6 oxidation state
PuO_2	plutonium (IV) dioxide
RH	remote handled
SEN4	EPA-mandated sensitivity study for CRA-2014
SI	saturation index
SIT	specific ion interaction theory
SO_4^{2-}	sulfate anion
TDB	Thermochemical Database
Th	thorium
Th^{4+}	thorium cation in the +4 oxidation state
Th(IV)	thorium in the +4 oxidation state
THEREDA	Thermodynamic Reference Database
TIC	total inorganic carbon
TRU	transuranic
U	uranium

UO_2^{2+}	uranyl ion
U(VI)	oxidized uranium
WDS	Waste Data System
WIPP	Waste Isolation Pilot Plant
WUF	waste unit factor

12 References

12.1 General References

Altmaier, M., C. Bube, C. Marquardt, V. Brendler, A. Richter, H.C. Moog, T. Scharge, W. Voigt, and S. Wilhelm, "THEREDA. Thermodynamic Reference Database. Summary of Final Report," Gesellschaft fuer Anlagen-und Reaktorsicherheit mbH (GRS), 2011 (No. GRS—265).

Altmaier, M., D. Fellhauer, X. Gaona, and E. Yancintas, "Assessment of Np(IV) and U(IV) as Improved Analogs for Pu(IV) in High Ionic Strength Brine Systems," Karlsruhe Institute of Technology Report, 2017.

Appelo, C.A.J., D. Postma, "Geochemistry, Groundwater and Pollution," Balkema Publishers, Amsterdam, The Netherlands, 2005.

Bethke, C. M., "The Geochemist's Workbench: A Users Guide to Rxn. Act2, Tact, React, and Gtplot," University of Illinois, Urbana-Champaign, IL, 213, 1994.

Day, B., "Reassessment of Need and Parameter Justification for Modeling Gas Generation Due To Radiolysis of Brine and Cellulose/Plastic/Rubber in WIPP for CRA-2019," Sandia National Laboratories, Carlsbad, NM, 2019 (ERMS 570873).

DOE (U.S. Department of Energy)., "Nuclear Physics and Reactor Theory, Volumes 1 and 2" *DOE Fundamentals Handbook*, US Department of Energy, Washington, DC, 1993.

DOE, *Title 40 CFR Part 191 Subparts B and C Compliance Recertification Application 2014, Appendix MgO-2014 Magnesium Oxide as an Engineered Barrier*, Carlsbad Field Office: Carlsbad, NM, 2014a.

DOE, *Title 40 CFR Part 191 Subparts B and C Compliance Recertification Application 2014, Appendix PA-2014 Magnesium Oxide as an Engineered Barrier*, Carlsbad Field Office: Carlsbad, NM, 2014b.

DOE, *Title 40 CFR Part 191 Subparts B and C Compliance Recertification Application 2014, Appendix PA, Attachment SOTERM*, Carlsbad Field Office: Carlsbad, NM, 2014c.

DOE, *Waste Isolation Pilot Plant Annual Site Environmental Report for 2016*, Carlsbad, NM: Carlsbad Field Office, 2017a (DOE-WIPP 17-3591).

DOE, *Waste Isolation Pilot Plant Annual Site Environmental Report for 2017 Revision 0*, Carlsbad Field Office: Carlsbad, NM, 2017b (DOE/WIPP 18-3591).

DOE, *Title 40 CFR Part 191 Subparts B and C Compliance Recertification Application 2014, Appendix PA, Attachment SOTERM*, Carlsbad Field Office: Carlsbad, NM, 2019a.

DOE, *Title 40 CFR Part 191 Subparts B and C Compliance Recertification Application 2014, Appendix PA, Attachment GEOCHEM*, Carlsbad Field Office: Carlsbad, NM, 2019b.

DOE, *Title 40 CFR Part 191 Compliance Recertification Application for Waste Isolation Pilot Plant (March), Appendix SCR,* Carlsbad, NM: Carlsbad Field Office, 2019c.

DOE, *Title 40 CFR Part 191 Subparts B and C Compliance Recertification Application 2014, Appendix PA, Attachment SOTERM*, Carlsbad Field Office: Carlsbad, NM, 2019d.

Domski, P., C. Sisk-Scott, "Prediction of Baseline Actinide Solubilities for CRA 2019 with an Updated EQ3/6 Pitzer Thermodynamic Database, DATA0.FM4," Sandia National Laboratories, Carlsbad, NM, 2019 (ERMS 571178).

EPA (U.S. Environmental Protection Agency), "40 CFR Part 194: Criteria for the Certification and Recertification of the Waste Isolation Pilot Plant's Compliance with the 40 CFR Part 191 Disposal Regulations," 61 *Federal Register*, 5223-5245, February 9, 1996.

EPA (U.S. Environmental Protection Agency), "Technical Support Document for Section 194.24: Evaluation of the Compliance Recertification Actinide Source Term, Backfill Efficacy and Culebra Dolomite Distribution Coefficient Values," Office of Radiation and Indoor Air, July 2017 (EPA-HQ-OAR-2014-0609).

Felmy, A.R., J. Weare, "The Prediction of Borate Mineral Equilibria in Natural Waters: Application to Searles Lake, California," *Geochimica et Cosmochimica Acta*, 50(12):2771-2783, 1986.

Gautier, Q., P. Bénézeth, V. Mavromatis, J. Schott, "Hydromagnesite Solubility Product and Growth Kinetics in Aqueous Solution from 25 to 75 C," *Geochimica et Cosmochimica Acta*, 138:1-20, 2014.

Giffaut, E., M. Grivé, P. Blanc, P. Vieillard, E. Colàs, H. Gailhanou, L. Duro, "Andra Thermodynamic Database for Performance Assessment: ThermoChimie," *Applied Geochemistry*, 49:225-236, 2014.

Gray, W.J., S.A. Simonson, "Gamma and Alpha Radiolysis of Salt Brines, PNL-SA-12746," 1984 Fall Meeting of the Materials Research Society, Boston, MA, 1984.

Grenthe, I., F. Mompean, K. Spahiu, H. Wanner, "Guidelines for the Extrapolation to Zero Ionic Strength, Version of 18 June 2013," OECD Nuclear Energy Agency, Data Bank, ISSY-les-Moulineaux, France, 2013.

Grivé, M., L. Duro, E. Colàs, E. Giffaut, "Thermodynamic Data Selection Applied to Radionuclides and Chemotoxic Elements: An Overview of the ThermoChimie-TDB," *Applied Geochemistry*, 55:85-94, 2015.

Guillaumont, R., J. Fanghänel, V. Neck, J. Fuger, D.A. Palmer, I. Grenthe, M.H. Rand, *Chemical Thermodynamics Vol. 5. Update on the Chemical Thermodynamics of Uranium, Neptunium, Plutonium, Americium and Technetium,* OECD, NEA-TDB, Amsterdam: Elsevier, 2003.

Hummel, W., G. Anderegg, I. Puigdomenech, L. Rao, O. Tochiyama, *Chemical Thermodynamics of Compounds and Complexes of U, Np, Pu, Am, Tc, Se, Ni and Zr with Selected Organic Ligands, Vol. 9*, Amsterdam: Elsevier, 2005.

Kitamura, A., K. Fujiwara, M. Mihara, M. Terashima, M. Yui, Y. Yoshida, "JAEA Thermodynamic Database for Performance Assessment of Geological Disposal of High-Level Radioactive and TRU Wastes," Japan Atomic Energy Agency, 2010, No. JAEA-DATA/CODE--2009-024.

Lemire, R.J., U. Berner, C. Musikas, D.A. Palmer, P. Taylor, O. Tochiyama, *Chemical Thermodynamics of Iron, Part 1*, Nuclear Energy Agency Data Bank, Organisation for Economic Co-operation and Development, Amsterdam: Elsevier Science Publishers B., V., 2013.

Lemire, R.J., J. Fuger, H. Nitsche, P.E. Potter, M.H. Rand, J. Rydberg, K. Spahiu, J.C. Sullivan, W.J. Ullman, P. Vitorge, H. Wanner, *Chemical Thermodynamics of Neptunium and Plutonium, Vol. 4*,

Nuclear Energy Agency Data Bank, Organisation for Economic Co-operation and Development, Amsterdam: Elsevier Science Publishers B. V., 2001.

Lemire, R.J., F. Garisto,. "The Solubility of U, Np, Pu, Th and Tc in a Geological Disposal Vault for Used Nuclear Fuel, Pinawa," Atomic Energy of Canada Limited, 1989 (Tech. Rep. AECL-10009).

Lorenz, J.C., "Assessment of the Potential for Karst in the Rustler Formation at the WIPP Site," Sandia National Laboratories, Carlsbad, New Mexico, 2006a (SAND2005-7303).

Lorenz, J.C., "Assessment of the Geological Evidence for Karst in the Rustler Formation at the WIPP Site," *Caves and Karst of Southeastern New Mexico,* In: In: Land, L., V.W. Lueth, W. Raatz, P. Boston, D.W. Love, eds., *New Mexico Geological Society Fall Field Conference Guidebook – 57Caves & Karst of Southeastern New Mexico*.

Martinez, J.S., E.F. Santillan, M. Bossant, D. Costa, M.E. Ragoussi. "The New Electronic Database of the NEA Thermochemical Database Project." *Applied Geochemistry*, 107:159-170, 2019.

National Academies of Sciences, Engineering, and Medicine. *Review of the Department of Energy's Plans for Disposal of Surplus Plutonium in the Waste Isolation Pilot Plant*, Washington, DC: The National Academies Press, 2020.

Offner, D. Private Communication, Response to Inquiry about MgO Content in the WIPP, Los Alamos National Laboratory, Carlsbad, NM, 2019 (Los Alamos Report LA-UR 19-28471).

Papenguth, H.W., Letter to Christine T. Stockman (Subject: Parameter Record Package for Colloidal Actinide Source Term Parameters, Attachment A: Rationale for Definition of Parameter Values for Humic Substances). Sandia National Laboratories: Carlsbad, NM, 1996a (ERMS 235855).

Papenguth, H.W., Y.K. Behl. "Test Plan for Evaluation of Colloid-Facilitated Actinide Transport at the Waste Isolation Pilot Plant (16 January)," Carlsbad, NM: Sandia National Laboratories, 1996b (TP 96-01. ERMS 417319).

Parkhurst, D.L., C.A.J. Appelo, *User's Guide to PHREEQC (Version 2): A Computer Program for Speciation, Batch-Reaction, One-Dimensional Transport, and Inverse Geochemical Calculations,* 1999.

Ragoussi, M.E., S. Brassinnes, "The NEA Thermochemical Database Project: 30 Years of Accomplishments," *Radiochimica Acta*, *103*(10):679-685, 2015.

Rai, D., D. Moore, K. Rosso, A. Felmy, H. Bolton, "Environmental mobility of Pu(IV) in the presence of Enthylenediaminetetraacetic acid: Myth or reality?" *Journal of Solution Chemistry,* 37: 957-986, 2008.

Rand, M., J. Fuger, I. Grenthe, V. Neck, D. Rai, *Chemical Thermodynamics of Thorium,* OECD, NEA-TDB, Amsterdam: Elsevier, 2008.

Rechard, R.P., "Improbability of TRU Waste Compaction by Salt Creep Causing Criticality in Bedded Salt Repository," Albuquerque, NM: Sandia National Laboratories, 2019 (ERMS 572199.).

Rechard, R.P., L.C. Sanchez, "Fissile Mass and Concentration Necessary for Criticality in Geologic Media near Bedded Salt Repository," Albuquerque, NM: Sandia National Laboratories, 2019 (ERMS 572195).

Rechard, R.P., E. Stein, "Hydrologic and Geochemical Constraints on Criticality in Geologic Media Near Bedded Salt Repository," Albuquerque, NM: Sandia National Laboratories, 2019 (ERMS 572191).

Roselle, G.T., “Determination of pCH+ Correction Factors in Brines,” Sandia National Laboratories, Carlsbad, NM, 2011 (ERMS 556699).

Sander, R., “Compilation of Henry’s Law Constants (version 4.0) for Water as Solvent.” *Atmospheric Chemistry and Physics*, 15:4399–4981, 2015.

Saylor, E.M., J.M. Scaglionie, “Nuclear Criticality Safety Assessment of Potential Plutonium Disposition at the Waste Isolation Pilot Plant,” Oak Ridge, TN: Oak Ridge National Laboratories, 2018.

Schramke, J.A., E.F.U. Santillan, R.T. Peake, “Plutonium Oxidation States in the Waste Isolation Pilot Plant Repository,” *Applied Geochemistry*, 116:104561, 2020.

Snoeyink, V.L., D. Jenkins, D. Jenkins, 1980. *Water Chemistry, Vol. 91*, New York: Wiley, 1980.

Stumm, W., J. J. Morgan, 1996. *Aquatic Chemistry,* New York: John Wiley & Sons, Inc., 1996.

Swanson, J.S., D.T. Reed, D.A. Ams, D.M. Norden, K.A. Simmons. 2012. *Status Report on the Microbial Characterization of Halite and Groundwater Samples from the WIPP*, Los Alamos National Laboratory, Carlsbad, New Mexico, 2012 (LCO-ACP-12, LA-UR 12-22824).

Turner, J.E, “Neutrons, Fission, and Criticality” In: *Atoms, Radiation, and Radiation Protection.* Wiley-VCH Verlag GmbH & Co. KGaA, Weinheim, Germany, 209-239, 2007.

Van Soest, G.D., *Performance Assessment Inventory Report—2018,* Los Alamos National Laboratory Carlsbad Operations, Carlsbad, New Mexico, 2018 (LA-UR-18-31882).

Wolery, T.J., *EQ3/6, A Software Package for Geochemical Modeling of Aqueous Systems: Package Overview and Installation Guide (Version 7.0),* Lawrence Livermore National Laboratory, Livermore, California, 1992*,* (UCRL-MA-110662 PT 1).